US CLIVAR Climate Variability & Predictability

VARIATIONS

doi:10.5065/D69Z93QF

Spring 2018 • Vol. 16, No. 2

Expansion of the Tropics

Guest Editors:
Kevin Grise[1] & Paul Staten[2]

[1]University of Virginia
[2]Indiana University

Within the last decade, a growing body of literature has concluded that Earth's tropical belt is expanding. While the tropics are often characterized by lush tropical vegetation, the edges of the tropics are home to some of the driest regions on the planet. This dichotomy of wet and dry regions reflects the atmosphere's Hadley circulation, with rising motion in the tropics and sinking motion in the subtropics. Global climate models indicate that a poleward expansion of the Hadley circulation is a robust characteristic of a warming climate, and many researchers have questioned whether the observed tropical expansion is driven by anthropogenic forcing. In fact, some studies have come to the conclusion that the expansion of the tropics is occurring at a faster rate than predicted by models. This is particularly concerning because a poleward expansion of the Hadley circulation suggests that subtropical dry regions will encroach upon increasingly populated regions.

Previous studies disagree on the magnitude, cause, and impacts of the recent tropical expansion.

New insights into tropical belt metrics

Nick A. Davis[1], Sean M. Davis[1], Darryn W. Waugh[2]

[1]University of Colorado Cooperative Institute for Research in Environmental Sciences (CIRES)/NOAA Earth System Research Laboratory
[2]Johns Hopkins University

While the Hadley cells have a profound impact on the surface climate of the tropical belt, measuring the areal extent of both has posed a decade-long challenge.

Sinking air at the edge of the Hadley cells warms and dries the subtropical atmosphere, leading to arid climates on land and stratocumulus decks over the oceans. This air is recirculated by the trade winds into the Intertropical Convergence Zone, evaporating ocean water along the way. There the water vapor condenses, releasing latent heat and driving the upward motion in the Hadley cells that brings frequent rain to the lush equatorial latitudes. While the latitudinal variation of sunlight drives the general circulation, it is the circulation itself that sculpts the varied climates of this tropical belt by redistributing heat and water vapor.

Climate model experiments suggest that the tropical belt and the Hadley cells are expanding poleward and will continue to expand in the future in response

IN THIS ISSUE

Part of this confusion stems from the lack of a standardized methodology. Another issue is whether studies consider the role of natural climate variability, in addition to the distinct roles of anthropogenic forcings such as well-mixed greenhouse gases, ozone, and aerosols. To address these issues, the US CLIVAR Working Group on the Changing Width of the Tropical Belt was formed in April 2016.

This edition of *Variations* highlights key contributions and findings related to the working group. Of particular emphasis is the need to standardize methodologies across studies. Another important point is that the recent tropical expansion is not just driven by anthropogenic forcing but also by coupled atmospheric-ocean variability and internal atmospheric variability. A final point is that tropical widening varies by region. On land, tropical expansion may be most strongly felt in Mediterranean climate zones. Over the ocean, tropical expansion will shift the subtropical highs, potentially impacting ocean upwelling zones and the biological productivity of important fisheries. These regional impacts of tropical expansion are only beginning to be understood.

US CLIVAR VARIATIONS

Editor:
Kristan Uhlenbrock
US CLIVAR Project Office
1201 New York Ave NW, Suite 400
Washington, DC 20005
202-787-1682 | usclivar.org

to radiative forcings (Seidel et al. 2008; Hu et al. 2013; Tao et al. 2015). However, previous estimates of this expansion have spanned an order of magnitude, ranging from a few tenths of a degree latitude per decade up to several degrees per decade. Narrowing the range of probable expansion rates is paramount for understanding the future of the Earth's climate, as minor shifts in the circulation could project strongly onto the large gradients in temperature, precipitation, and cloud cover at the belt's edges (Birner et al. 2014). An important component of such research is assessing the ability of climate models to simulate realistic trends and variability in the latitude of the Hadley cell edge.

Directly measuring the Hadley cell is a difficult endeavor, unfortunately, as there are insufficient *in situ* wind observations to construct a reliable estimate of the mean meridional circulation (Waliser et al. 1999). Instead, researchers have been forced to identify other observable structures that could be used as proxies for the Hadley cell edges. One popular metric is the latitude of the tropopause break in the subtropics, which separates the warm tropical upper-tropospheric air within the Hadley cell from the cold air in the lower stratosphere (Seidel and Randel 2007). Another popular metric is the subtropical jet latitude, which is connected to the Hadley cell through zonal momentum dynamics (Archer and Caldeira 2008; Fu and Lin 2011). Sea level pressure (SLP) and surface zonal winds have been used as proxies for the location of sinking and diverging air at the cells' edges (Choi et al. 2014), along with various features of outgoing longwave radiation (OLR; Hu and Fu 2007), precipitation minus evaporation (P-E; Lu et al. 2007), and total column ozone (Hudson 2012). A subset of these tropical width metrics and their associated physical fields are shown in Figure 1. We do not examine metrics based on ozone, as they are not robust and probably more related to stratospheric dynamics than tropical belt variability (Davis et al. 2018).
Recent progress

This potluck of metrics presents a conundrum: studies disagree on the observed rate of expansion, and many metrics give different estimates of tropical expansion even in the same reanalysis or climate model simulation (Davis and Rosenlof 2012). The outcome of a recent Chapman Conference on this topic was a call to explore these metrics to more deeply understand what they measure, how they agree or disagree, and why (Heffernan 2016; Davis et al. 2016).

A subgroup of the US CLIVAR Changing Width of the Tropical Belt Working Group was convened to provide guidance on which metrics are most appropriate to quantify key impacts of the changing width of the tropical belt. Two studies were published by members in the nascent stage of the working group — Solomon et al. (2016) and Davis and Birner (2017). Solomon (2016) examined the interannual relationships among metrics within a large ensemble of simulations by a single

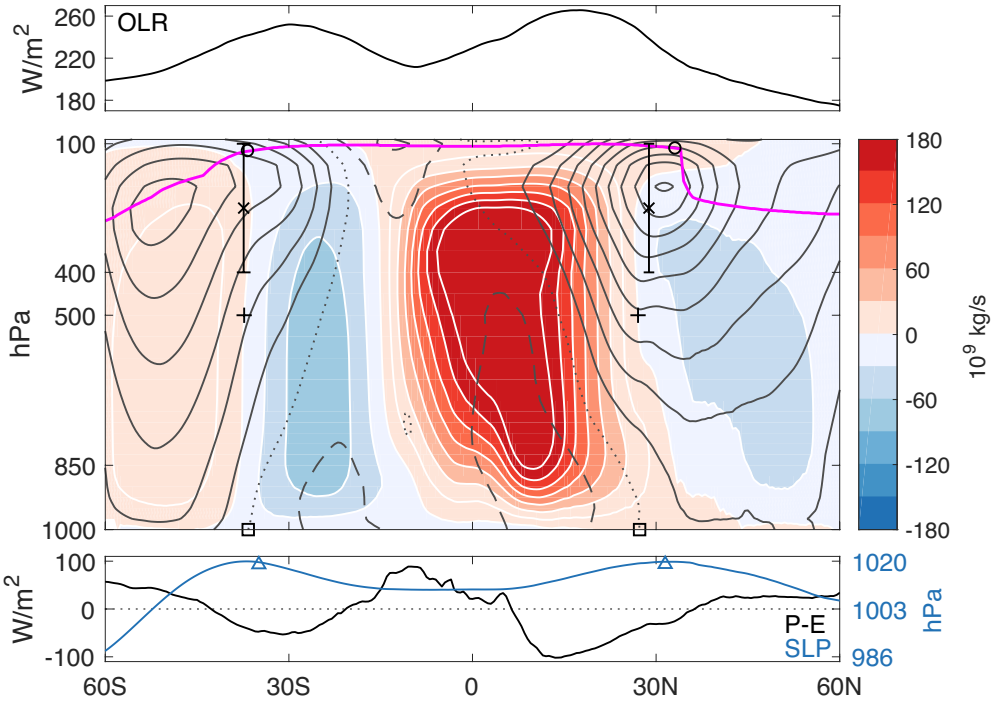

Figure 1. Zonal-mean climate in February 2000 from the MERRA2 reanalysis. (Top panel) OLR in W/m^2; (middle panel) mean meridional streamfunction in shading (10^9 kg/s), with positive values indicating a clockwise circulation, positive (solid line) and negative (dashed line) zonal-mean zonal wind every 5 m/s, with the zero contour dotted, and tropopause pressure in magenta; (bottom panel) P-E in W/m^2 (black line) and SLP in hPa (blue line). Tropical belt metrics examined here include the tropopause break latitudes (circles), the subtropical jet latitudes (x's), the Hadley cell edge latitudes (+), the latitudes of zero surface zonal wind (squares), and the latitudes of the subtropical ridge (triangles).

model and reanalyses, while Davis and Birner (2017) examined the month-to-month relationships among metrics in different models and reanalyses. However, the particular metrics and simulations examined as well as the timescales of interest differed sufficiently that a follow-up study was warranted.

Relationships among the metrics

Authored by members of the working group and currently in review, Waugh et al. (2018) evaluates a representative subset of tropical belt width metrics with 23 preindustrial control climate model simulations from the Coupled Model Intercomparison Project Phase 5 (CMIP5; Taylor et al. 2012). These simulations provide self-consistent representations of large-scale dynamics and, unlike reanalyses, are not subject to unphysical discontinuities or trends due to observational inhomogeneities and changes in data coverage. Also, nearly all of the metrics chosen for this study are objective, avoiding the use of arbitrary levels or subjective thresholds, which can influence the derived trends (Birner 2010). For simplicity, the particular focus of this article is on metrics of the dynamics rather than on metrics of the impacts: the Hadley cell edge latitude, defined by the zero contour of the 500 hPa mean meridional streamfunction; the latitude of the subtropical ridge, defined as the maximum in SLP; the latitude of zero surface zonal wind; the latitude of the subtropical jet, defined as the maximum in the 100 to 400 hPa average zonal-mean zonal wind with the surface wind subtracted; and the latitude of the tropopause break, defined by the maximum gradient in tropopause pressure (Figure 1). We will briefly comment on OLR and P-E, as these are also widely used.

A basic measure of how the metrics relate are their interannual correlations, illustrated here as a heat map for the annual mean (Figure 2). Each correlation reflects the multi-model-mean correlation between two metrics' edge latitudes in one hemisphere. Corroborating the

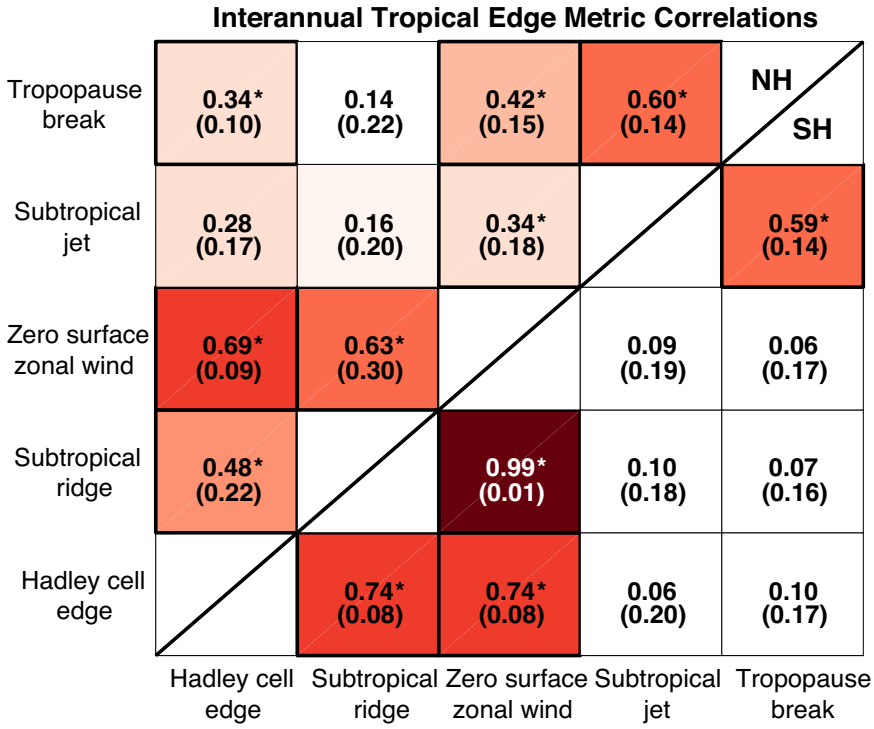

Figure 2. Multi-model-mean interannual correlations between annual mean tropical belt edge metrics in the Northern (NH) and Southern (SH) Hemispheres from 23 preindustrial control climate model simulations. The standard deviation of the correlations is shown in parentheses. If at least 20 models have a significant correlation, the box is outlined in bold and noted with a star.

results of Solomon (2016) and Davis and Birner (2017), there are two clusters of metrics, within which metrics are correlated and between which there are weak or insignificant correlations. On the one hand, the Hadley cell edge latitude, the latitude of zero surface zonal wind, and the latitude of the subtropical ridge are correlated in both hemispheres. On the other hand, the subtropical jet and tropopause break latitudes are correlated in both hemispheres. While there are some minor correlations across these sets of metrics in the Northern Hemisphere, the distinction between the two sets is decisive in the Southern Hemisphere.

Consistent with these interannual relationships and confirming the results of the Solomon et al. and David and Birner findings, in both hemispheres trends in the subtropical jet and tropopause break latitudes are weakly correlated, if at all, with trends in the Hadley cell edge latitude, while trends in the latitudes of the subtropical ridge and zero surface zonal wind are highly correlated with trends in the Hadley cell edge latitude (Waugh et al. 2018).

One noteworthy exception is the relationship between the subtropical ridge and the Hadley cell edge in the Northern Hemisphere. The predominance of landmasses in the Northern Hemisphere concentrates the subtropical ridge into oceanic centers of action, whereas it is more zonally symmetric in the Southern Hemisphere. In the Northern Hemisphere, the projection of zonal-mean Hadley cell variability is, thus, limited to the ocean basins, and the correlation with the zonal-mean subtropical ridge is weaker (Schmidt and Grise 2017).

Why aren't all the metrics related?

A valid concern is that these findings seem to undermine the physics that motivated some of the metrics, such as the latitude of the subtropical jet. However, it is worth examining the projection of Hadley cell variability onto the underlying physical fields to see whether this is the case (Figure 3).

Poleward shifts of the Hadley cell are associated with weakened upper tropospheric westerlies in the tropics and subtropics (Figure 3a), consistent with the weakened temperature gradients that accompany Hadley circulation variability and change (Lu et al. 2008; Adam et al. 2014). These wind anomalies do not project onto the maximum in the upper-tropospheric westerlies, though, so they are not associated with a shift in the jet. Instead, the subtropical jet latitude is more related to variability in the strength of the Hadley cell, while eddy-driven jet and mid-latitude wave variability is associated with variability in the Hadley cell edge latitude (Staten and Reichler 2014; Gotor and Zapato-Álvarez 2018). These two orthogonal patterns of variability may simply result from the subtropical jet shielding the tropics from mid-latitude waves.

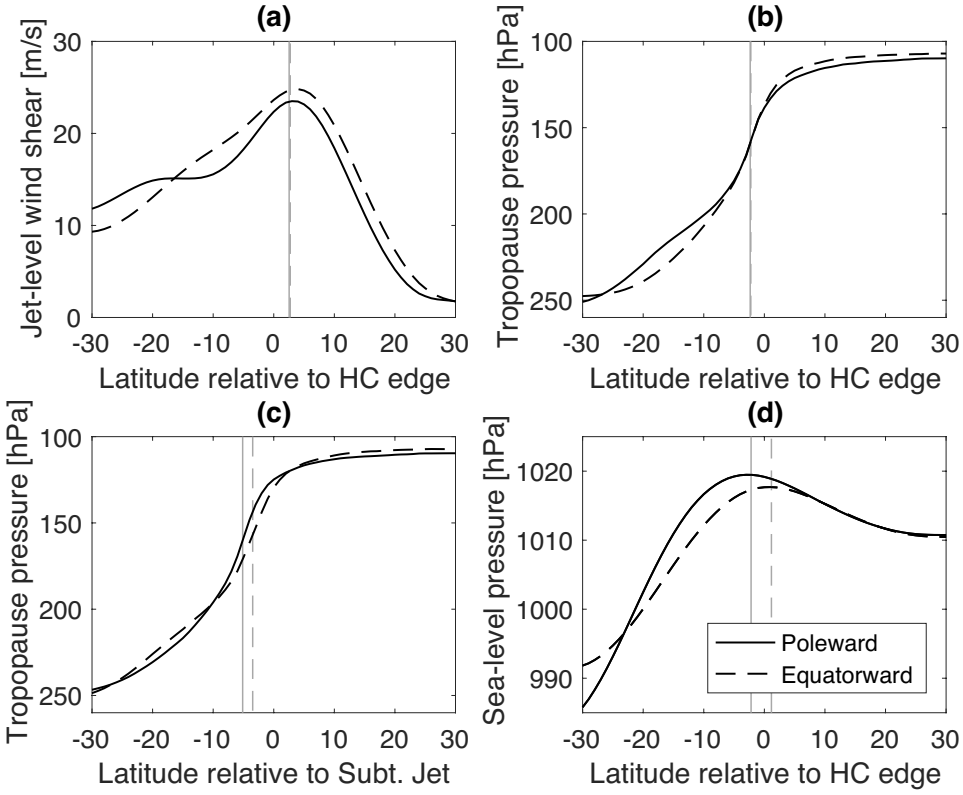

Figure 3. Projection of a 2 (a, d) or 10 (b, c) standard deviation poleward (solid curve) and equatorward (dashed curve) shift of the Southern Hemisphere Hadley cell edge onto (a) the jet-level wind with the surface wind removed, (b) the tropopause pressure, and (d) SLP. (c) As in (b) except for a shift of the subtropical jet. Poleward is to the left. Solid (dashed) vertical lines denote the poleward (equatorward) tropical edge metric latitudes.

Concurrent with the poleward shift of the Hadley cell edge is a weakening of the tropopause height differential between the tropics and extratropics, with no corresponding projection onto the tropopause break latitude (Figure 3b). Instead, it is poleward shifts of the subtropical jet that are associated with poleward shifts of the tropopause break (Figure 3c), as might be expected through thermal wind balance.

Increasing SLP follows poleward shifts in the Hadley cell edge (Figure 3d) as the divergent surface flow must follow the region of subsidence. While not shown, the surface zonal wind pattern also reflects this change in SLP as the latitude of zero surface zonal wind follows the Hadley cell edge latitude (Solomon et al. 2016; Davis and Birner 2017).

The tropopause break latitude is related to the subtropical jet latitude but only weakly. How can this be reconciled with the finding that the jet projects onto tropopause height variability? It is possible that double-tropopauses confound the metric itself, as these typically occur in the

subtropics in the vicinity of the jet (Manney et al. 2017). A further consideration is that while the zonal wind field is continuous and smoothly varying, the tropopause break is not. It may be harder to track its true variability, especially in the zonal mean.

Numerous tropical belt metrics are based on the meridional gradient of OLR and various features of P-E (see Figure 1). While not direct measurements of the Hadley cells, OLR and P-E integrate the energetic impacts of the cells and may provide useful information about their variability. However, perhaps because these fields are also impacted by clouds, water vapor, atmospheric composition, and surface processes, their connection to trends in the Hadley cell edges is not robust. Studies disagree on whether OLR metrics are useful proxies for the Hadley cell edges, in part because different OLR metrics measure different aspects of OLR variability (Solomon et al. 2016; Mantsis et al. 2017; Waugh et al. 2018). It also appears that OLR trends may be driven more by cloud feedbacks than by circulation changes (Donohoe et al. 2014; Waugh et al. 2018). Similarly, the response of P-E to radiative forcings reflects slow thermodynamic changes while the circulation responds more rapidly (Grise and Polvani 2017). Despite their promise, the OLR and P-E responses to radiative forcings are impacted enough by other processes to preclude their use as metrics for examining trends in the Hadley cell edges. While a given field may vary with the Hadley cell edge, the field and any metrics based upon it do not necessarily shift with the edge.

Conclusions

Waugh et al. (2018) generally corroborates the main conclusions of the Solomon (2016) and Davis and Birner (2017) studies, namely:

- The subtropical jet latitude and tropopause break latitude are poorly correlated, if at all, with the latitude of the Hadley cell edge.
- The surface zonal circulation is highly correlated with the latitude of the Hadley cell edge.

Regarding the second conclusion, Davis and Birner (2017; and previously Choi et al. 2014) suggest that the eddy momentum forcing on the zonal flow binds the meridional overturning circulation to the surface wind stress. Similarly, to ensure mass continuity, the subsidence at the edge of the Hadley cell must be co-located with the subtropical ridge where the sinking air diverges at the surface. The maximum in subsidence, however, is located equatorward of the Hadley cell edge and is weakly correlated with the edge in the Northern Hemisphere (Davis and Birner 2017). This may be one factor, in addition to land-ocean asymmetries, that leads to the unexpectedly weak correlation between the subtropical ridge and the Hadley cell edge in the Northern Hemisphere.

While the results here seem to suggest that conventional tropopause metrics are unrelated to the Hadley cell edge latitude, it would be imprudent to suggest that this is the case for all possible tropopause metrics. There is some evidence that the tropopause height, or at least its gradient from the equator to the subtropics, may have some relationship with the Hadley cell width (Amaya et al. 2017).

Given the pitfalls of defining tropical belt width metrics, a key finding of this working group is that new metrics, or metrics untested by Waugh et al. (2018), Solomon et al. (2016), or Davis and Birner (2017), should be evaluated against the Hadley cell edge latitude in model simulations or reanalyses to ensure that the chosen metric is, in fact, related to the Hadley cell edge latitude. As these studies have shown, both the surface zonal wind and SLP could be reasonable observational proxies, with a few exceptions. The use of metrics with better observational constraints may allow for the investigation of tropical width variability further back in time and with greater reliability.

References

Amaya, D. J., N. Siler, S-P Xie, and A. J. Miller, 2017: The interplay of internal and forced modes of Hadley cell expansion: lessons from the global warming hiatus. *Climate Dyn.*, **9**, 1–15, doi:10.1007/s00382-017-3921-5.

Archer, C. L. and K. Caldeira, 2008: Historical trends in the jet streams. *Geophys. Res. Lett.*, **35**, doi:10.1029/2008GL033614.

Birner, T., 2010:. Recent widening of the tropical belt from global tropopause statistics: Sensitivities. *J. Geophys. Res. Atmos.*, **115**, doi:10.1029/2010JD014664.

Birner, T., S. M. Davis, and D. J. Seidel, 2014: The changing width of Earth's tropical belt. *Phys. Today*, **67**, 38–44, doi:10.1063/PT.3.2620.

Choi, J., S.-W. Son, J. Lu, and S.-K. Min, 2014: Further observational evidence of Hadley cell widening in the Southern Hemisphere. *Geophys. Res. Lett.*, **41**, 2590–2597, doi:10.1002/2014GL059426.

Davis, N. A., and T. Birner, 2017: On the discrepancies in tropical belt expansion between reanalyses and climate models and among tropical belt width metrics. *J. Climate*, **30**, 1211–1231, doi:10.1175/JCLI-D-16-0371.1.

Davis, S. M. and K. H. Rosenlof, 2012: A multidiagnostic intercomparison of tropical-width time series using reanalyses and satellite observations. *J. Climate*, **25**, 1061–1078, doi:10.1175/JCLI- D-11-00127.1.

Davis, S. M., T. Birner, and D. Seidel, 2016: How do climate variations affect the width of the tropics? *Eos*, **97**, doi:10.1029/2016EO049309.

Davis, S. M., B. Hassler, and K. H. Rosenlof, 2018: Revisiting ozone measurements as an indicator of tropical width. *Prog. Earth Plan. Sci.*, submitted.

Donohoe, A., K. C. Armour, A. G. Pendergrass, and D. S. Battisti, 2014: Shortwave and longwave radiative contributions to global warming under increasing CO2. *Proc. Nat. Acad. Sci.*, **111**, 16700–16705, doi:10.1073/pnas.141290111.

Fu, Q. and P. Lin, 2011: Poleward shift of subtropical jets inferred from satellite-observed lower stratospheric temperatures. *J. Climate*, **24**, 5597–5603, doi:10.1175/JCLI-D-11-00027.1.

Grise, K. M., and L. M. Polvani, 2017: Understanding the time scales of the tropospheric circulation response to abrupt CO2 forcing in the Southern Hemisphere: Seasonality and the role of the stratosphere. *J. Climate*, **30**, 8497–8515, doi:10.1175/JCLI-D-16-0849.1.

Heffernan, O., 2016: The mystery of the expanding tropics. *Nature*, **530**, 20–22, doi:10.1038/530020a.

Hu, Y. and Q. Fu, 2007: Observed poleward expansion of the Hadley circulation since 1979. *Atmos. Chem. Phys.*, **7**, 5229–5236, doi:10.5194/acp-7-5229-2007.

Hu, Y., L. Tao, and J. Liu, 2013: Poleward expansion of the Hadley circulation in CMIP5 simulations. *Adv. Atmos. Sci.*, **30**, 790, doi:10.1007/s00376-012-2187-4.

Hudson, R. D., 2012: Measurements of the movement of the jet streams at mid-latitudes, in the Northern and Southern Hemispheres, 1979 to 2010. *Atmos. Chem. Phys.*, **12**, 7797–7808, doi:10.5194/acp-12-7797-2012.

Lu, J., G. A. Vecchi, and T. Reichler, 2007: Expansion of the Hadley cell under global warming. *Geophys. Res. Lett.*, **118**, doi:10.1029/2006GL028443.

Manney, G. L., and Coauthors, 2017: Reanalysis comparisons of upper tropospheric–lower stratospheric jets and multiple tropopauses. *Atmos. Chem. Phys.*, **17**, 11541–11566, doi:10.5194/acp-17-11541-2017.

Mantsis, D. F., S. Sherwood, R. Allen, and L. Shi, 2017: Natural variations of tropical width and recent trends. *Geophys. Res. Lett.*, **44**, 3825–3832, doi:10.1002/2016GL072097.

Schmidt, D. F., and K. M. Grise, 2017: The response of local precipitation and sea level pressure to Hadley cell expansion. *Geophys. Res. Lett.*, **44**, 10573–10582, doi:10.1002/2017GL075380.

Seidel, D. J. and W. J. Randel, 2007: Recent widening of the tropical belt: Evidence from tropopause observations. *J. Geophys. Res.*, **112**, doi:10.1029/2007JD008861.

Seidel, D. J., Q. Fu, W. J. Randel, and T. J. Reichler, 2008: Widening of the tropical belt in a changing climate. *Nat. Geosci.*, **1**, 21–24, doi:10.1038/ngeo.2007.38.

Solomon, A., L. M. Polvani, D. W. Waugh, and S. M. Davis, 2016: Contrasting upper and lower atmospheric metrics of tropical expansion in the Southern Hemisphere. *Geophys. Res. Lett.*, **43**, 10,496–10,503, doi:10.1002/2016GL070917.

Tao, L., Y. Hu, and J. Liu, 2015: Anthropogenic forcing on the Hadley circulation in CMIP5 simulations. *Climate Dyn.*, **46**, 3337–3350, doi:10.1007/s00382-015-2772-1.

Taylor, K. E., R. Stouffer, and G. A. Meehl, 2012: An overview of CMIP5 and the experiment design. *Bull. Amer. Meteor. Soc.*, **93**, 285–298, doi:10.1175/BAMS-D-11-00094.1.

Waliser, D. E., Z. Shi, J. R. Lanzante,and A. H. Oort, 1999: The Hadley circulation: assessing NCEP/NCAR reanalysis and spare in-situ estimates. *Climate Dyn.*, **15**, 719, doi:10.1007/s003820050312.

Waugh, D. W., and Coauthors, 2018: Revisiting the relationship among metrics of tropical expansion. *J. Climate*, submitted.

Zurita-Gotor, P. and P. Álvarez-Zapatero, 2018: Coupled interannual variability of the Hadley and Ferrel cells. *J. Climate*, doi:10.1175/JCLI-D-17-0752.1.

The importance of ENSO/PDO to recent tropical widening

Robert J. Allen[1] and Dillon J. Amaya[2]

[1]University of California, Riverside
[2]Scripps Institution of Oceanography, University of California, San Diego

Understanding the primary drivers of tropical widening has been a major focus of recent literature, with studies showing the importance of anthropogenic factors, including greenhouse gases (Lu et al. 2007, 2009; Tao et al. 2016), stratospheric ozone depletion (Son et al. 2009; Polvani et al. 2011; Waugh et al. 2015), and anthropogenic aerosols (Allen et al. 2012a,b, 2014; Kovilakam and Mahajan 2015; Allen and Ajoku 2016). Several recent studies have also shown the importance of natural climate variability, including unforced internal atmospheric variability (Garfinkel et al. 2015), as well as the coupled ocean-atmosphere variability that drives prominent modes of naturally occurring sea surface temperature (SST) variability (Grassi et al. 2012; Nguyen et al. 2013; Allen et al. 2014; Adam at el. 2014; Lucas and Nguyen 2015; Amaya et al. 2017; Mantsis et al 2017; Allen and Kovilakam 2017). As an example of the latter, the tropical belt contracts during warm El Niño-Southern Oscillation (ENSO) events but expands during cold ENSO (La Niña) events (Lu et al. 2008). Similar conclusions are obtained for the warm (cold) phase of the Pacific Decadal Oscillation (PDO), which has an El Niño (La Niña)-like SST pattern (Grassi et al. 2012; Allen et al. 2014).

Several analyses have expanded on these initial findings and have shown the importance of recent ENSO/PDO evolution to tropical widening. Mantsis et al. (2017) show the maximum 20-year tropical widening signal, based on satellite estimates of outgoing longwave radiation, occurred during 1993–2012 and is associated with a cold ENSO/PDO pattern. Using Community Atmosphere Model version 5 (CAM5; Neale et al., 2012) coupled ocean-atmosphere "pacemaker" simulations, which feature observed central to eastern tropical Pacific SSTs (Kosaka and Xie 2013), Allen and Kovilakam (2017) find more than double the rate of tropical widening compared to fully coupled simulations. Amaya et al. (2017) use statistical techniques to identify anthropogenic and internal modes of tropical width variability. The forced mode is related to Earth's radiative imbalance and exhibits an increasing trend over the 20th century; whereas, the internal mode is ENSO-like. They draw interesting parallels between tropical widening and the recent "hiatus" in global warming, due to the hiatus also representing a similar interaction between forced and internal variability (Kosaka and Xie 2013). Amaya et al. (2017) show that the superposition of their internal and forced modes has resulted in an acceleration of tropical widening while simultaneously producing a slowdown in global warming, illustrating the important modulation of forced trends by internal variability (Figure 1). Furthermore, relatively large, multi-decadal tropical expansion in coupled ocean-atmosphere control simulations (i.e., without external forcing) is associated with the cold phase of ENSO/PDO (Allen and Kovilakam 2017; Mantsis et al. 2017). Here, we emphasize results from Allen and Kovilakam (2017), which show the change in the phase of ENSO/PDO during the late 1990s (from positive to negative) has likely played a significant role in recent widening of the tropical belt, particularly in the Northern Hemisphere.

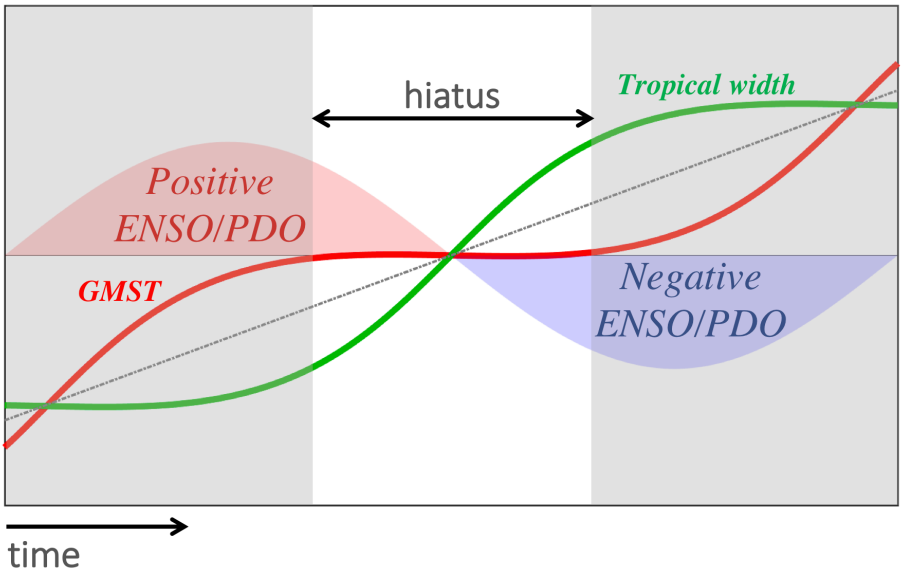

Figure 1. Schematic demonstrating the interplay between anthropogenic forcings (gray dashed line) and different phases of Pacific SST variability (red/blue sine wave). Green line represents trajectory of a tropical width index. Red line represents trajectory of measured global mean surface temperature (GMST) with time. During the transition from a positive PDO (red shading) to a negative PDO (blue shading), forced global warming is dampened and the trend flattens out, producing a hiatus period. Simultaneously, the increasing prevalence of La Niña-like forced tropical expansion drives accelerated widening of the tropics through an enhancement of the externally forced component.

Data and approach

We focus on one (dynamical) annual mean metric of tropical width that is commonly used throughout the literature, the latitude where the mean meridional circulation at 500 hPa becomes zero on the poleward side of the subtropical maximum. See Davis et al. in this issue for the advantages and disadvantages of selecting this or any other particular index. Changes in tropical width (expansion/contraction) are estimated by taking a least-squares trend of the annual mean mean meridional circulation time series. Widening of the tropical belt is represented by positive trends in the Northern Hemisphere and negative trends in the Southern Hemisphere. Trend uncertainty, which accounts for trend robustness across realizations, is estimated as twice the standard error. In other cases (e.g., uncertainty in a given realization's trend), trend significance is based on a standard t-test, accounting for the influence of serial correlation by using the effective sample size (Wilks 1995).

Observation-based meridional winds (for mean meridional circulation calculations) come from seven reanalyses, including NCEP/NCAR (R1; Kalnay et al. 1996), NCEP-DOE (R2; Kanamitsu et al. 2002), ERA-Interim (Dee et al. 2011), MERRA (Rienecker et al. 2011), CFSR (Saha et al. 2010), 20CR (Compo et al. 2011), and JRA-55 (Kobayashi et al. 2015).

We use 35 coupled ocean-atmosphere realizations from the Community Earth System Model (CESM) Large Ensemble Community Project (Kay et al. 2015; referred to as CAM5 CMIP in this article). These simulations are run at 0.9°x1.25° resolution and extended from 2005 to 2014 using RCP8.5. Each realization is identically forced; the only difference is the initial condition, which allows the assessment of natural climate variability. Note that the ensemble mean averages out natural climate variability and, thus, represents the forced response.

CAM5 atmosphere-only (AMIP) simulations, which are forced with the real-world evolution of SSTs and sea ice, are conducted at 1.9°x2.5° resolution over the 1970–2014 time period. Time-varying forcing follows the Coupled Model Intercomparison Project Phase 5 (CMIP5) (Taylor et al., 2012) dataset (using RCP4.5 after 2005) and includes solar variability; estimated concentrations of greenhouse gases, ozone, and volcanic aerosols; and primary emissions of sulfur dioxide, and black and organic carbon. All CAM5 results are based on 10

ensemble members, and we analyze the 1979–2014 time period. Each member is integrated from an independent initial condition, which is obtained by applying a random surface temperature perturbation in the year 1970.

We assume the observed SST evolution can be decomposed into a forced SST and an unforced SST component. The forced component is obtained from the ensemble mean SSTs from 25 CMIP5 coupled ocean-atmosphere models. Implicitly, we are assuming the models accurately simulate the true forced signal. The forced SST component from 1979–2014 is neither El Niño- nor La Niña-like. Uncertainty exists in whether or not the tropical Pacific will become more El Niño-like with continued warming (which includes enhanced warming of the tropical eastern Pacific and a slow down of the tropical Pacific Walker circulation). If the true forced signal from 1979 to present is more El Niño-like than what the models simulate, then that would imply a larger tropical contraction signal from the forced SST component (Lu et al. 2008). Therefore, natural SST variability would lead to a larger tropical widening contribution than what we show. If, however, the true forced signal from 1979 to present is more La Niña-like than what the models simulate, then this would imply a stronger tropical expansion signal from the forced SSTs. Thus, natural SST variability would lead to weaker widening than what we show.

The unforced component is estimated by removing the forced SST trend from the observed SST at each grid point. This is done by estimating the 1979–2014 forced SST as the least square trend from monthly anomalies at each grid point. This monthly regression coefficient is then used to get an estimate of the forced SST, which is subtracted from the observed SST. We perform additional CAM5 AMIP experiments with fixed external forcing and replace the SST field with either the estimated forced or unforced evolution. To isolate the effects of SSTs only, we also fix the sea ice in these simulations (to a repeating monthly climatology based on the first year of simulation). CAM5 forced and unforced SST shows the role of SST evolution on tropical widening, including the relative roles of externally forced and unforced SST evolution.

The importance of unforced SST variability

Figure 2 shows 1979–2014 Northern and Southern Hemisphere annual mean tropical widening histograms based on coupled ocean-atmosphere (red; CAM5 CMIP) and atmosphere-only simulations driven by observed SSTs (blue; CAM5 AMIP), as well as estimates from seven different reanalyses (black X's). Reanalyses show

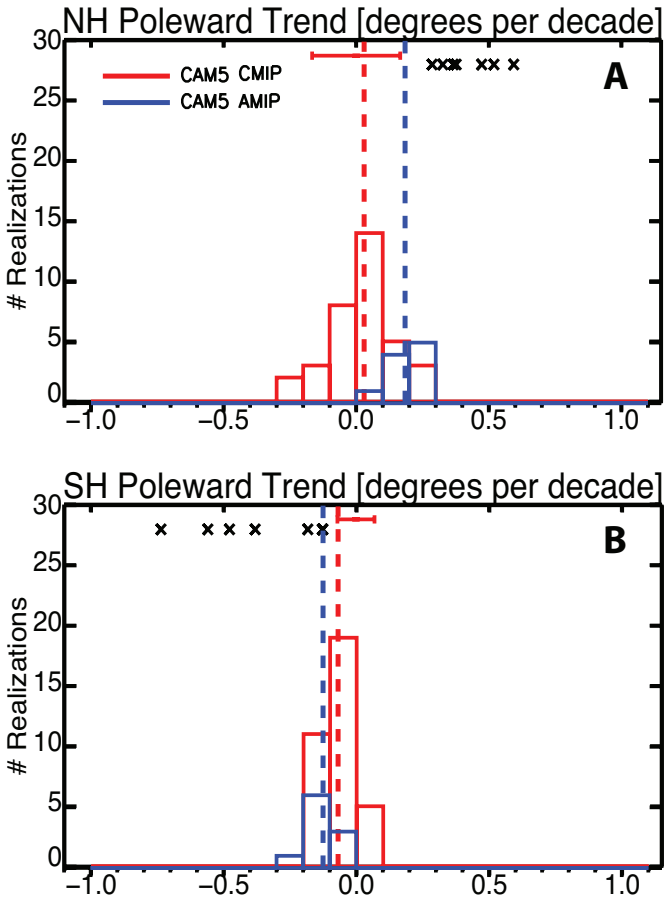

Figure 2. 1979–2014 CAM5 annual mean meridional circulation tropical expansion histograms. Northern (top panels) and Southern (bottom panels) Hemisphere tropical widening trends for coupled ocean-atmosphere CAM5 simulations from the Large Ensemble Project (CAM5 CMIP; red) and atmosphere-only CAM5 simulations (CAM5 AMIP; blue). Vertical dashed lines represent the ensemble mean trend for CAM5 CMIP (red) and CAM5 AMIP (blue). Tropical widening rates from seven reanalyses are also included (black X's). Widening of the northern (southern) tropical belt is indicated by positive (negative) trends. Also included is the 90% confidence range of 36-year tropical widening trends from CAM5's preindustrial control experiment (red horizontal line). Units are degrees latitude per decade.

a considerable spread, ranging from 0.30 to 0.60° per decade in the Northern Hemisphere and -0.70 to -0.10° per decade in the Southern Hemisphere. This highlights the large uncertainty in observational/reanalysis-based estimates of recent tropical widening (Davis et al. 2012, Garfinkel et al. 2015). Nonetheless, the reanalysis mean shows significant poleward displacement of the Northern and Southern Hemisphere tropical edges at 0.42 and -0.37° per decade, respectively.

CAM5 CMIP and CAM5 AMIP experiments also yield a large range of tropical widening trends. This implies natural climate variability, including both internal atmospheric variability and natural SST variability, significantly contributes to the large range of simulated trends. Recall that AMIP simulations are forced with identical, real-world SST evolution, implying that the large range of AMIP trends is due to internal atmospheric variability, as opposed to SST variability. Furthermore, some model realizations capture the magnitude of observed tropical widening, especially in the case of CAM5 AMIP.

Figure 2 also shows that the ensemble mean CAM5 AMIP signal is larger than the ensemble mean CAM5 CMIP signal and in better agreement to the observations, particularly in the Northern Hemisphere. For example, the CAM5 CMIP ensemble mean Northern Hemisphere widening is 0.03 ± 0.04° per decade compared to the CAM5 AMIP mean of 0.18 ± 0.04° per decade. Since the same model is used for the CMIP and AMIP ensemble mean and the ensemble mean largely averages out natural climate variability, the different rates of widening between the coupled ocean-atmosphere model and atmosphere-only model are not due to model (dynamical cores, parameterizations, etc.) or forcing differences, but are likely related to the real-world evolution of SSTs.

The observed SSTs have both a forced component due to anthropogenic emissions, volcanic eruptions, and solar variability, and an unforced component due to

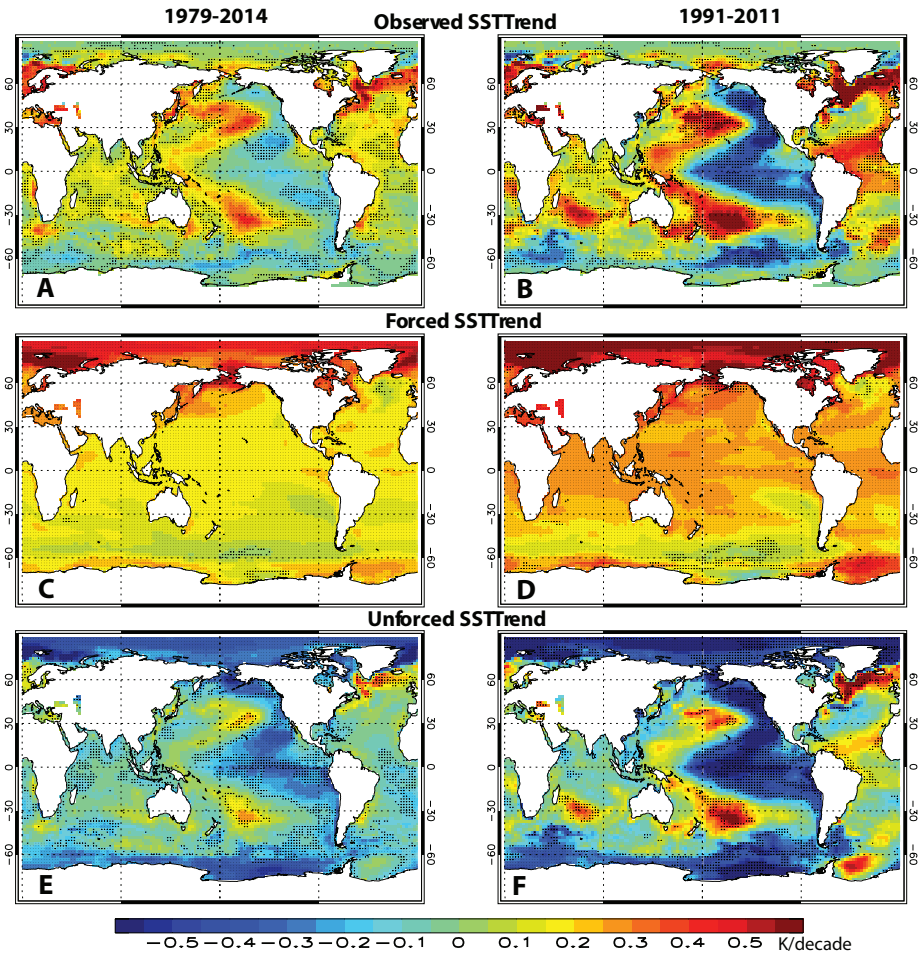

Figure 3. 1979–2014 and 1991–2011 SST trends. (a, b) Hadley Centre observed SST trends; (c, d) the forced component, estimated from the ensemble mean of the CMIP5 20th century all forcing experiments, combined with RCP4.5; and (e, f) the unforced component, which is estimated by removing the forced SST trend from the observed SST at each grid point. Left panels show the trend from 1979–2014. Right panels show the trend from 1991–2011, when the rate of tropical widening is largest. This shorter, 21-year time period also corresponds to the maximum trend (toward the cold ENSO phase) in the Southern Oscillation Index and the PDO. Trend symbols represent significance at the 90% (diamond); 95% (x); and 99% (dot) confidence level, accounting for autocorrelation. Units are K per decade.

natural variability. As discussed in the above section, we assume the observed SST evolution can be decomposed into its forced and unforced SST components (Figure 3). We note that the unforced SST trend pattern resembles the observations throughout the Pacific, including cooling of the tropical eastern and central Pacific, and an off-equatorial boomerang-like shaped warming in the western and central Pacific (i.e., a cold ENSO/PDO-like pattern). This is particularly prominent for the time period 1991–2011, when the cold ENSO/PDO-like SST pattern is exceptionally strong. In contrast, the forced SST trend pattern, which shows large-scale relatively uniform warming, bears little resemblance to the observed SST trends. We also note that unforced SST bears several similarities to the SST pattern associated with tropical widening, which also resembles a cold ENSO/PDO-like SST pattern. These results alone suggest that the importance of observed SSTs to recent tropical widening is unlikely related to the forced component.

To test this hypothesis, we perform a 10-member ensemble of CAM5 AMIP experiments with fixed external forcing and replace the observed SST dataset with either the forced or unforced contribution. Figure 4 shows Northern and Southern Hemisphere rates of tropical widening based on reanalyses, and CAM5 forced and unforced SST. Consistent with prior results, a large range of trends exists for both CAM forced and unforced SST, due to internal atmospheric variability. However, Figure 4 shows that CAM5 forced SST yields weaker ensemble mean rates of tropical widening. The ensemble mean CAM5 forced SST mean meridional circulation trends are not significant, at 0.02° per decade in the Northern Hemisphere and -0.03° per decade in the Southern Hemisphere. The corresponding trends from CAM5 unforced SST are much larger (particularly in the Northern Hemisphere), and significant at 0.18° and -0.05° per decade, respectively. These results show the importance of the unforced component of the real-world evolution of SSTs to recent tropical widening.

Comparing the ensemble mean CAM5 unforced SST tropical widening trends (which provide an estimate of the unforced SST contribution) to those from the coupled ocean-atmosphere experiments from CMIP5 and CAM5 CMIP (which provide an estimate of the total forced contribution), we find that the unforced SSTs drive the bulk of recent tropical widening, especially

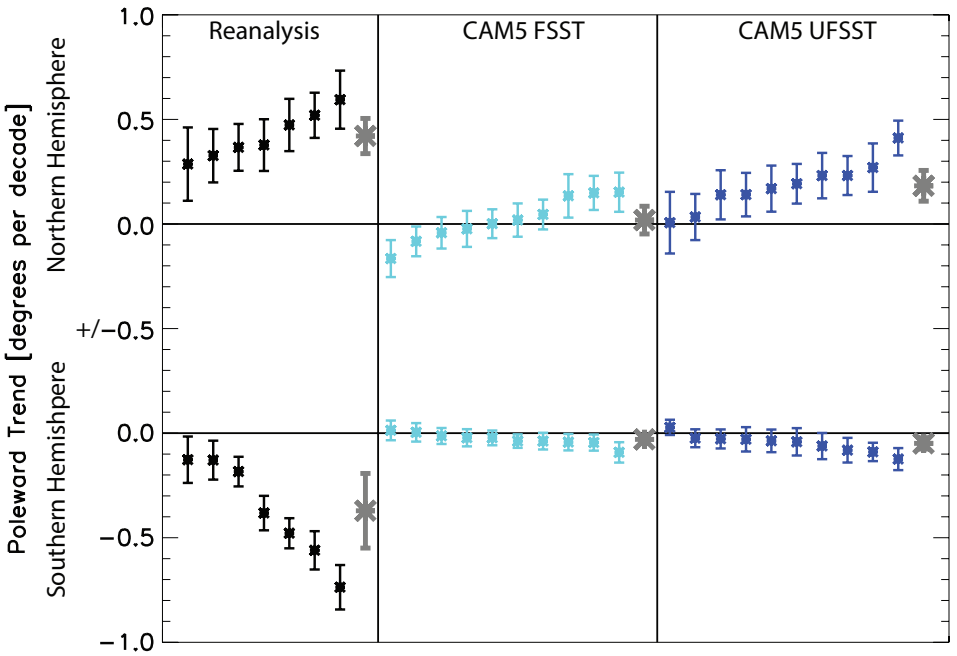

Figure 4. 1979–2014 annual mean meridional circulation tropical expansion for individual realizations. Trends are shown for the Northern (top set of lines) and Southern (bottom set of lines) Hemisphere for seven reanalysis (black), ten CAM5 AMIP fixed external forcing simulations driven by the forced (CAM5 FSST; cyan) and the unforced (CAM5 UFSST; blue) evolution of SSTs. Also included for each data source is the corresponding ensemble mean (thick gray). Individual trend uncertainty is based on a standard t-test, accounting for the influence of serial correlation by using the effective sample size. Uncertainty in the ensemble mean trend is estimated as twice the standard error. Units are degrees latitude per decade.

in the Northern Hemisphere (not shown). Natural SST variability yields more than double the rate of total (Northern + Southern Hemisphere) tropical widening relative to the forced contribution. The importance of natural SST variability in driving Northern Hemisphere tropical widening is particularly robust — the CAM5 unforced SST mean meridional circulation trends are nearly an order of magnitude larger than those based on the forced signal. Thus, natural SST variability associated with ENSO/PDO accounts for the bulk of recent tropical widening, particularly in the Northern Hemisphere.

We conclude by noting that anthropogenic forcing will likely become more important through the 21st century. However, our results imply that any future, anthropogenically forced tropical widening signal will be significantly modulated by natural climate variability associated with ENSO/PDO evolution (as illustrated by Figure 1). We also note that in the near future, tropical widening is likely to slow down, as the PDO/ENSO cycle transitions to the opposite phase.

References

Adam, O., T. Schneider, and N. Harnik, 2014: Role of changes in mean temperatures versus temperature gradients in the recent widening of the Hadley circulation. *J. Climate*, **27**, 7450–7461, doi:10.1175/JCLI-D-14-00140.1.

Allen, R. J., S. C. Sherwood, J. R. Norris, and C. S. Zender, 2012a: The equilibrium response to idealized thermal forcings in a comprehensive GCM: Implications for recent tropical expansion. *Atmos. Chem. Phys*., **12**, 4795–4816, doi:10.5194/acp-12-4795-2012.

Allen, R. J., S. C. Sherwood, J. R. Norris, and C. S. Zender, 2012b: Recent Northern Hemisphere tropical expansion primarily driven by black carbon and tropospheric ozone. *Nature*, **485**, 350–354, doi:10.1038/ nature11097.

Allen, R. J., J. R. Norris, and M. Kovilakam, 2014: Influence of anthropogenic aerosols and the Pacific Decadal Oscillation of tropical belt width. *Nature Geosci*., **7**, 270–274, doi:10.1038/ ngeo2091.

Allen, R. J., and O. Ajoku, 2016: Future aerosol reduction and widening of the northern tropical belt. *J. Geophys. Res. Atmos*., **121**, 6765–6786, doi:10.1002/2016JD024803.

Allen, R. J., and M. Kovilakam, 2017: The role of natural climate variability in recent tropical expansion. *J. Climate,* **30** , 6329–6350, doi:10.1175/JCLI-D-16-0735.1

Amaya, D. J., N. Siler, S. Xie, and A. J. Miller, 2017: The interplay of internal and forced modes of Hadley Cell expansion: lessons from the global warming hiatus. *Climate Dyn.,* doi:10.1007/s00382-017-3921-5.

Compo, G., and Coauthors, 2011: The Twentieth Century Reanalysis Project. *Quart. J. Roy. Meteor. Soc.*, **137**, 1–28, doi:10.1002/qj.776.

Davis, S. M., and K. H. Rosenlof, 2012: A multidiagnostic intercomparison of tropical-width time series using reanalyses and satellite observations. *J. Climate*, **25**, 1061–1078, doi:10.1175/ JCLI-D-11-00127.1.

Dee, D. P., and Coauthors, 2011: The ERA-Interim reanalysis: Configuration and performance of the data assimilation system. *Quart. J. Roy. Meteor. Soc*., **137**, 553–597, doi:10.1002/ qj.828.

Garfinkel, C. I., D. W. Waugh, and L. M. Polvani, 2015: Recent Hadley cell expansion: The role of internal atmospheric variability in reconciling modeled and observed trends. *Geophys. Res. Lett.*, **42**, 10,824–10,831, doi:10.1002/2015GL066942.

Grassi, B., G. Redaelli, P. Canziani, and G. Visconti, 2012: Effects of the PDO phase on the tropical belt width. *J. Climate*, **25**, 3282–3290, doi:10.1175/JCLI-D-11-00244.1.

Kalnay, E., and Coauthors, 1996: The NCEP/NCAR 40-year reanalysis project. *Bull. Amer. Meteor. Soc.,* **77**, 437–471, doi:10.1175/1520-0477(1996)077,0437:TNYRP.2.0.CO;2

Kanamitsu, M., W. Ebisuzaki, J. Woollen, S.-K. Yang, J. J. Hnilo, M. Fiorino, and G. L. Potter, 2002: NCEP–DOE AMIP-II Reanalysis (R-2). *Bull. Amer. Meteor. Soc*., **83**, 1631–1643, doi:10.1175/BAMS-83-11-1631.

Kay, J. E., and Coauthors, 2015: The Community Earth System Model (CESM) Large Ensemble Project: A community resource for studying climate change in the presence of internal climate variability. *Bull. Amer. Meteor. Soc*., **96**, 1333–1349, doi:10.1175/ BAMS-D-13-00255.1.

Kobayashi, S., and Coauthors, 2015: The JRA-55 Reanalysis: General specifications and basic characteristics. *J. Meteor. Soc. Japan*, **93**, 5–48, doi:10.2151/jmsj.2015-001.

Kosaka, Y., and S.-P. Xie, 2013: Recent global-warming hiatus tied to equatorial Pacific surface cooling. *Nature*, **501**, 403–408, doi:10.1038/nature12534.

Kovilakam, M., and S. Mahajan, 2015: Black carbon aerosol induced Northern Hemisphere tropical expansion. *Geophys. Res. Lett*., **42**, 4964–4972, doi:10.1002/2015GL064559.

Lu, J., G. A. Vecchi, and T. Reichler, 2007: Expansion of the Hadley cell under global warming. *Geophys. Res. Lett*., **34**, doi:10.1029/2006GL028443.

Lu, J., G. Chen, and D. M. W. Frierson, 2008: Response of the zonal mean atmospheric circulation to El Niño versus global warming. *J. Climate*, **21**, 5835–5851, doi:10.1175/2008JCLI2200.1.

Lu, J., C. Deser, and T. Reichler, 2009: Cause of the widening of the tropical belt since 1958. *Geophys. Res. Lett*., **36**, doi:10.1029/2008GL036076.

Lucas, C., B. Timbal, and H. Nguyen, 2014: The expanding tropics: A critical assessment of the observational and modeling studies. *Wiley Interdiscip. Rev.: Climate Change*, **5**, 89–112, doi:10.1002/wcc.251.

Mantsis, D. F., S. Sherwood, R. J. Allen, and L. Shi, 2017: Natural variations of tropical width and recent trends. *Geophys. Res. Lett.,* **44**, 3825–3832, doi:10.1002/2016GL072097.

Neale, R. B., and Coauthors, 2012: Description of the NCAR Community Atmosphere Model (CAM 5.0). *NCAR Tech. Note,* NCAR/TN-4861STR, 274 pp.

Nguyen, H., A. Evans, C. Lucas, I. Smith, and B. Timbal, 2013: The Hadley circulation in reanalyses: Climatology, variability, and change. *J. Climate*, **26**, 3357–3376, doi:10.1175/JCLI-D-12-00224.1.

Polvani, L. M., D. W. Waugh, G. J. P. Correa, and S.-W. Son, 2011: Stratospheric ozone depletion: The main driver of twentieth-century atmospheric circulation changes in the Southern Hemisphere. *J. Climate,* **24**, 795–812, doi:10.1175/ 2010JCLI3772.1.

Rienecker, M. M., and Coauthors, 2011: MERRA: NASA's Modern- Era Retrospective Analysis for Research and Applications*. J. Climate*, **24**, 3624–3648, doi:10.1175/JCLI-D-11-00015.1.

Saha, S., and Coauthors, 2010: The NCEP Climate Forecast System Reanalysis. *Bull. Amer. Meteor. Soc.,* **91**, 1015–1057, doi:10.1175/2010BAMS3001.1.

Son, S.-W., N. F. Tandon, L. M. Polvani, and D. W. Waugh, 2009: Ozone hole and Southern Hemisphere climate change. *Geophys. Res. Lett*., **36**, doi:10.1029/2009GL038671.

Tao, L., Y. Hu, and J. Liu, 2016: Anthropogenic forcing on the Hadley circulation in CMIP5 simulations. *Climate Dyn*., **46**, 3337–3350, doi:10.1007/s00382-015-2772-1

Taylor, K. E., R. J. Stouffer, and G. A. Meehl, 2012: An overview of CMIP5 and the experiment design*. Bull. Amer. Meteor. Soc*., **93**, 485–498, doi:10.1175/BAMS-D-11-00094.1.

Waugh, D. W., C. I. Garfinkel, and L. M. Polvani, 2015: Drivers of recent tropical expansion in the Southern Hemisphere: Changing SSTs or ozone depletion? *J. Climate*, **28**, 6581–6586, doi:10.1175/JCLI-D-15-0138.1

Wilks, D. S., 1995: Statistical methods in the atmospheric sciences. *Academic Press*, 467 pp., ISBN:9780123850232.

Natural variability in the width of the tropics

Isla Simpson

National Center for Atmospheric Research

Roughly a decade ago, it was realized that in the approximately 30 years since satellite records began the tropics, as measured by various climatological definitions, had been expanding, raising concern as to whether this was an externally forced trend arising from anthropogenic forcings such as increasing greenhouse gas concentrations (e.g., Seidel et al. 2008). While our theoretical expectations and numerical climate model simulations indeed predict that the tropics should expand as the planet warms (Frierson et al. 2007; Lu et al. 2007; Tao et al; 2016), it has now become acknowledged that natural, internal variability has likely played an important role in the expansion that has been observed over recent decades (Quan et al. 2014; Garfinkel et al. 2015; Mantsis et al. 2016; Amaya et al. 2017; Allen and Kovilakam 2017). Over the observational record, the confounding influences of natural variability and external forcings make a quantitative assessment of the magnitude of forced trends extremely challenging, if not impossible. As we wait for our observational record to lengthen and forced trends to emerge (or not), we must maintain an appreciation of the influence of natural variability on what we have seen and what we may see in the future.

There are a number of ways in which to define the width of the tropics (Davis and Rosenlof 2012; Waugh et al. 2018; Davis et al. this issue) and a number of approaches (e.g., seasons, trend lengths) that could be used to characterize variability and change, all of which cannot be covered here. Readers, however, can refer to a number of studies that have used a variety of metrics and approaches to investigate natural variability in tropical width (Kang et al. 2013; Quan et al. 2014; Garfinkel et al. 2015; Allen and Kovilakam 2017; Amaya et al. 2017; Quan et al, 2018). Here, natural variability in tropical width will be illustrated with three examples: the annual mean

width (i.e., difference between the Northern Hemisphere and Southern Hemisphere tropical edges); the latitude of the Northern Hemisphere edge during winter (December-January-February average (DJF)); and the latitude of the Southern Hemisphere edge during summer (DJF). The edge of the tropics will be defined here as the latitude of transition of near surface winds from easterly to westerly (e.g., Adam et al. 2018).

Figure 1 illustrates the challenge that we face in isolating the forced response from natural variability and even in simply characterizing the variability over our observational record. Annual mean tropical width for a variety of reanalysis products is shown in Figure 1a. The two products that cover the entire 20th century show strong disagreement in the earlier part of the record, indicating that we do not have a constrained observational record of tropical width that extends much before the beginning of the satellite era (around 1979). While differences do exist, the agreement is better after 1979 (see also Nguyen et al. 2013), and therefore the following analysis will focus on the variability in the 38-year period between 1980 and 2017.

Since 1980, the annual mean width of the tropics has fluctuated interannually with a standard deviation (σ) of ~0.8°–1° latitude (Figure 1c), with individual years typically varying within an ~4° latitude range (~4σ, Figure 1a). Figure 1b illustrates similar time series but for 40 members of a large ensemble of simulations performed with the Community Earth System Model, version 1 (CESM1, Kay et al. 2015), referred to as LENS hereafter. All 40 simulations are run under an identical forcing scenario (see Figure 1 caption) and differ only in a round-off level perturbation introduced to the surface temperature field in 1920. Thus, the differences between ensemble members arise only from internal ocean-atmosphere variability. From 1980 to 2017, CESM exhibits comparable

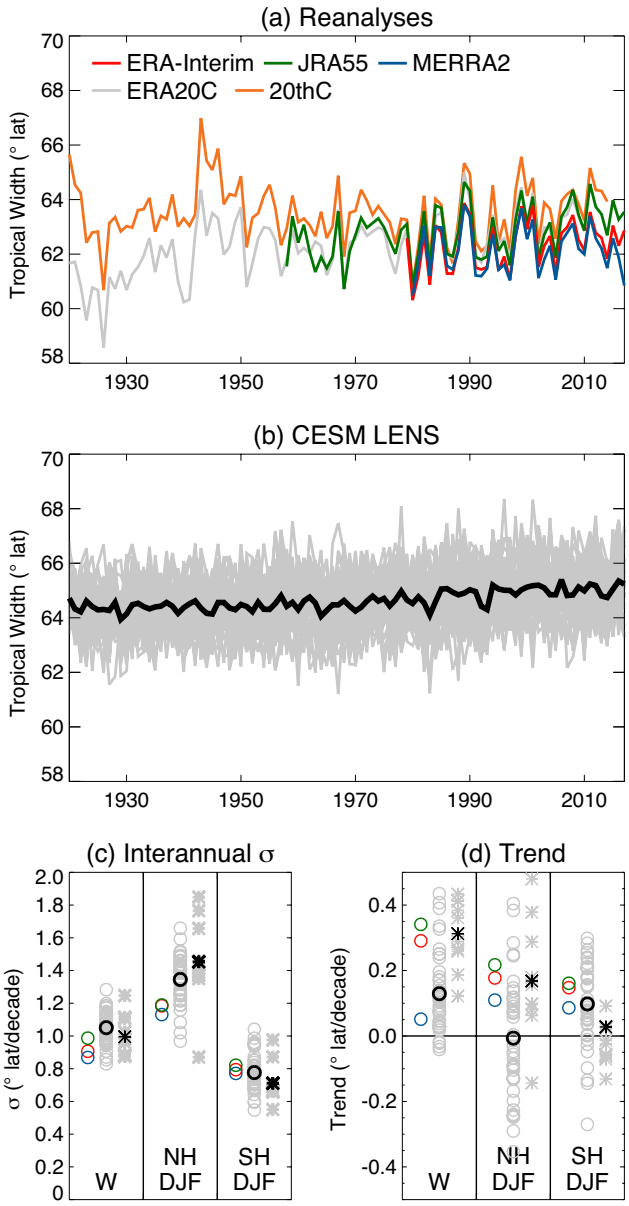

Figure 1. (a) Time series of annual mean tropical width for five different reanalyses: ERA-Interim (Dee et al 2011), JRA55 (Kobayashi et al 2015), MERRA2 (Gelaro et al 2017), ERA20C (Poli et al 2016), 20th century reanalysis (20thC; Compo et al. 2011). (b) Time series of annual mean tropical width from the CESM LENS (grey=individual members, black=ensemble mean). The LENS is run under CMIP5 historical forcings prior to 2006 and under the RCP8.5 scenario thereafter. (c) Interannual standard deviation, σ, of the annual mean width, the NH DJF edge and the SH DJF edge calculated using 1980–2017 for the three more strongly constrained reanalyses (ERA-Interim (red), JRA55 (green), MERRA2 (blue)), the CESM LENS (grey circles) and CESM simulations run with the same forcings as LENS, but with observed SSTs prescribed at the lower boundary (grey asterisks). (d) is as (c) but for the linear trends from 1980-2017. The colors in panels (c) and (d) correspond to those in (a) and (b) and note that zonal wind at 10 m is used for the reanalyses while the zonal wind at the lowest model level is used for CESM.

interannual variability to observations (Figure 1c). But the LENS makes clear that even our assessment of interannual variability over a 38-year record is subject to considerable uncertainty since individual members are characterized by an annual mean tropical width σ of anywhere between 0.8° and 1.3° latitude.

Between 1980 and the present, ERA-Interim (Dee et al. 2011) and JRA-55 (Kobayashi et al. 2015) reanalyses have exhibited an annual mean widening trend of around 0.3° per decade (Figure 1d, see also Lucas et al. 2014 and references therein). MERRA2 (Gelaro et al. 2017) exhibits a considerably weaker trend, but there may be reasons to be concerned about the ability of MERRA2 to constrain the divergent tropical circulation (DeWeaver and Nigam 1997). The ensemble mean trend of the CESM LENS, which can be considered to be the externally forced trend in CESM, is only around 0.13° per decade. The wide range of trends exhibited by individual members, however, indicates the dominant role that natural variability can play over a 38-year record. Individual members are characterized by trends of anywhere between 0.04° per decade and 0.43° per decade, which illustrates the importance of comparing the observations with a large number of model simulations that span the range of possible outcomes that could arise as a result of the combined influences of external forcing and natural variability (Garfinkel et al. 2015). The presence of external forcings has clearly weighted the CESM simulations toward exhibiting a widening trend in the annual mean, but the wide range of behaviors seen in individual members demonstrates the challenges in quantifying the forced trend in our one observed record.

Even if the presence of internal variability renders our estimation of the forced trend in the real world highly uncertain, can we at least conclude that the trends that have been observed are outside of the expectations from natural variability alone? To provide an indication of this, we can compare with the trends that are present in unforced preindustrial control (piControl) simulations. This comparison is made in Figure 2 using 22 piControl simulations from the Coupled Model Intercomparison Project Phase 5 (CMIP5), along with an 1800 year long piControl simulation that accompanies the CESM LENS. For annual mean tropical width and the Northern Hemisphere DJF tropical edge, the majority of the CMIP5 models exhibit interannual variability that is comparable with observations (Figure 2a,c). The discrepancy between models and reanalyses is slightly greater in the Southern Hemisphere DJF, which may relate to common biases in the Southern Hemisphere jet stream (which is often biased equatorward) and Southern Annular Mode behavior (which is often overly persistent) (Kidston and Gerber 2010; Simpson and Polvani 2016). Nevertheless, roughly half of the CMIP5 models and CESM exhibit interannual variability in the Southern Hemisphere DJF tropical edge that is comparable with reanalyses. Figures 2b,d,f illustrate the range of possible trends that could be obtained from 38-year segments of these piControl simulations (black bars). For annual mean tropical width, the ERA-Interim and JRA55 trends lie outside of the distribution of trends found in the piControl simulations of almost all the models, indicating that, to the extent we can trust the representation of long term natural variability in the models, the observed trends in annual mean tropical width are extremely unlikely to have arisen from natural variability alone (consistent with the tendency of the forced LENS simulations to produce a tropical widening (Figure 1d)). The same cannot be said for the DJF Northern and Southern Hemisphere trends. While the reanalyses indicate a poleward migration of the Northern and Southern Hemisphere tropical edges during DJF, these trends are not outside of the realms of what natural variability can produce. While there is good reason to believe that stratospheric ozone depletion has contributed to an expansion of the tropics in the Southern Hemisphere during DJF (Polvani et al 2011; McLandress et al 2011; Garfinkel et al. 2015; Waugh et al 2015; Solomon and Polvani 2016), consistent with the fact that the forced CESM LENS does show a poleward expansion in the ensemble mean (Figure 1d), this has not been sufficient to give rise to an observed trend that is larger than could arise from natural variability alone. In the Northern Hemisphere DJF, the fact that the reanalysis trends lie within the expectations from natural variability

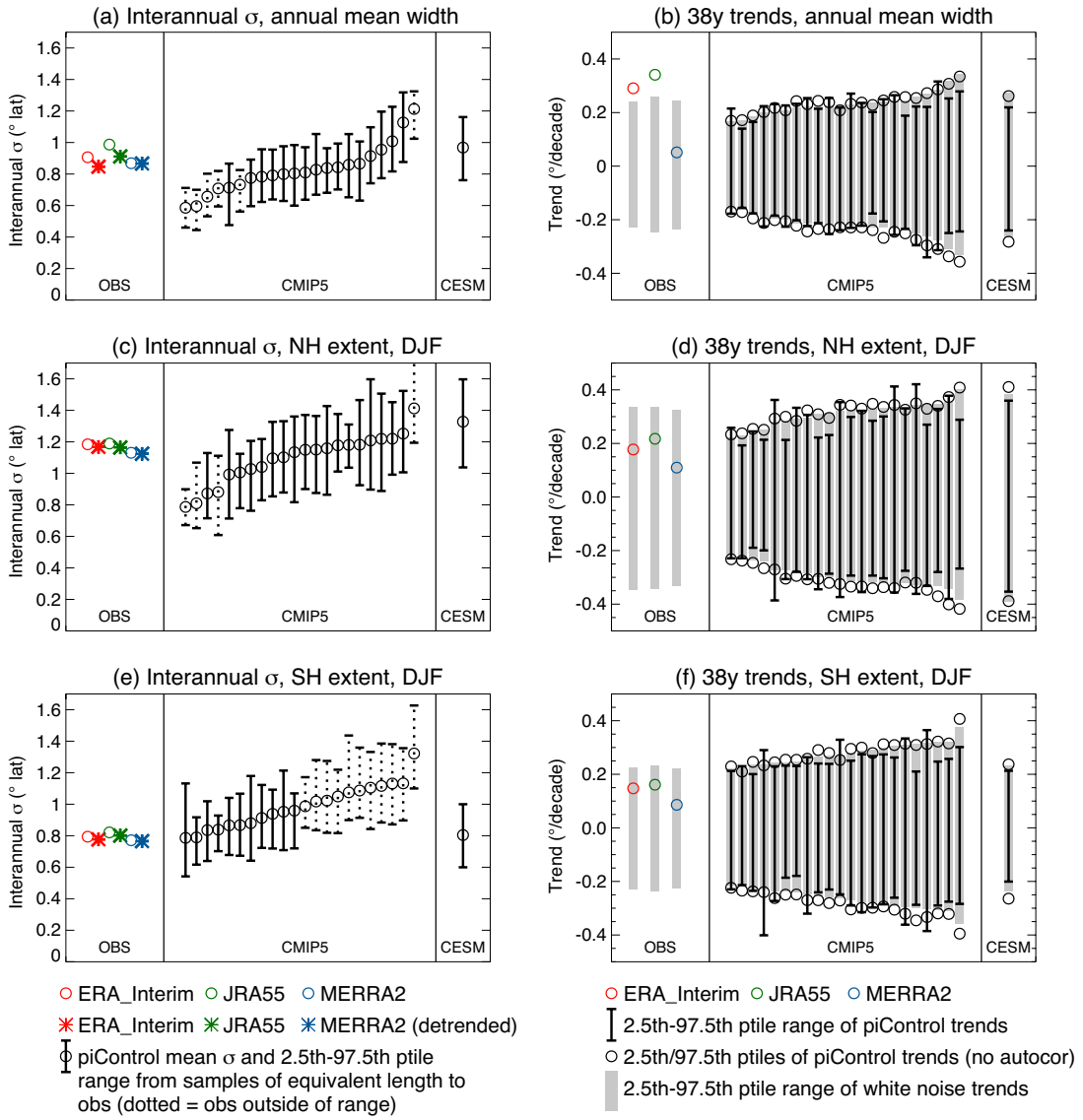

Figure 2. (top) Annual mean tropical width, (middle) Northern Hemisphere DJF tropical edge, (bottom) Southern Hemisphere DJF tropical edge. (left) Interannual standard deviation (σ) for the reanalyses (1980–2017) both before and after detrending, for CMIP5 piControl simulations from 22 models, and for a piControl simulation with CESM. Black circles depict the mean σ calculated from all years of simulation and the error bars depict the 2.5 to 97.5 percentile range of σ's estimated from overlapping segments of length 38 years from the piControl simulations. 2.5 to 97.5 percentile ranges that do not encompass the observed value are shown by dotted lines. (right) Trends from 1980-2017 for the reanalyses along with the 2.5 to 97.5 percentile range of trends obtained from overlapping 38-year segments of the piControl simulations (black error bars). Black circles depict the 2.5 and 97.5 percentiles of trends obtained from 1000, 38-year time series obtained by picking individual years at random from the piControl simulation i.e., removing any autocorrelation from the time series due to slow processes. Grey bars depict the 2.5 to 97.5 percentile range of trends obtained from 1000, 38-year samples of synthetic time series generated using Gaussian white noise with an interannual σ equal to that of the respective reanalysis (detrended) or simulation. Note that for DJF, a record length of 38 years means 37 DJF seasons are used to calculate σ and the trend. The CMIP5 piControl simulation lengths range from 255 to 1000 years, and the CESM piControl simulation is 1800 years long.

is consistent with the results from the forced LENS simulations, which show no forced trend over this time period (Figure 1d).

What then is the nature of this natural variability? Many studies have discussed the important role of the El Niño-Southern Oscillation (ENSO) and the Pacific Decadal Oscillation (PDO) in contributing to observed trends, particularly for the Northern Hemisphere (Grassi et al. 2012; Garfinkel et al. 2015; Mantsis et al. 2016; Allen and Kovilakam 2017; Amaya et al; 2017) with cold ENSO/PDO phases being characterized by a wider tropical belt (see also Allen et al. this issue). Indeed, it can be seen in Figure 1d that the ensemble mean of 10 CESM simulations with prescribed historical SSTs as opposed to a coupled ocean (gray asterisks) exhibits a greater expansion of the Northern Hemisphere tropics during DJF. However, ambiguity remains over whether decadal modes of variability in the ocean are actually required to explain the trends or whether the apparent decadal influence of the ocean simply arises from the chance sampling of individual years characterized by different ENSO states. An appropriate null hypothesis to consider is that the trends that arise due to internal variability do so simply as a result of the chance sampling of individual years with no underlying correlation from one year to the next. Can we distinguish the variability from this possibility? The answer is no. In Figure 2b, this is tested in two different ways for the piControl simulations. The first is just by using a bootstrapping methodology where individual years from the piControl simulation are randomly sampled and then strung together so that, by construction, there is no correlation from one year to the next. An assessment of the range of 38-year trends that can be obtained from such samples is shown by the black circles that accompany the piControl trend ranges in Figure 2b,d,f. These indicate that the actual trends simulated by the models are consistent with the chance sampling of individual years with no correlation from one year to the next. The second test takes this a step further and assumes that the variability in tropical width is given by a Gaussian white noise distribution characterized by the interannual σ. The gray bars in Figure 2b,d,f indicate that the trends simulated by the models are consistent with this representation of the variability. We, therefore, have no indication from the models that their internal variability is anything more than the chance sampling of year-to-year fluctuations with one year being unrelated to the next. While multidecadal modes of variability in the ocean could play a role, this it not necessary to explain the long-term trends that arise due to natural variability in the models. Building on this model analysis, if we then assume that the observed atmosphere displays internal variability that is simply represented by Gaussian white noise with σ equal to the observed interannual σ, then it can be seen that random sampling of this noise can give rise to 38-year trends as large as 0.25° per decade in the annual mean width, 0.33° per decade in Northern Hemisphere DJF extent and 0.23° per decade in Southern Hemisphere DJF extent (gray bars in Figure 2b,d,f). The actual observed annual mean width trend lies outside of this range, but the Northern and Southern Hemisphere DJF trends do not.

The asterisks in Figure 1d make clear that even without differences in SST variability, the sampling of atmospheric noise can give rise to a wide range of trends. The relative roles of atmosphere-only variability and coupled ocean-atmosphere variability can be assessed more quantitatively within CESM by comparison of the coupled piControl simulation with a control simulation with prescribed climatological SSTs derived from the coupled simulation (Figure 3). Certainly, ocean variability is required to explain the full range of interannual variability that is seen in the coupled simulation, but variability that is internal to the atmosphere is actually a dominant contribution. The interannual σ found in the climatological SST simulation is around 72% of that in the coupled simulation for annual mean tropical width, 78% for the Northern Hemisphere DJF edge, and 84% for the Southern Hemisphere DJF edge. Furthermore, upon regressing out the contribution to interannual variability that is linearly related to ENSO in the coupled simulation (via the Nino3.4 index), the σ of tropical width/extent is reduced to similar values to those of the climatological SST simulation (compare filled circles and asterisks in

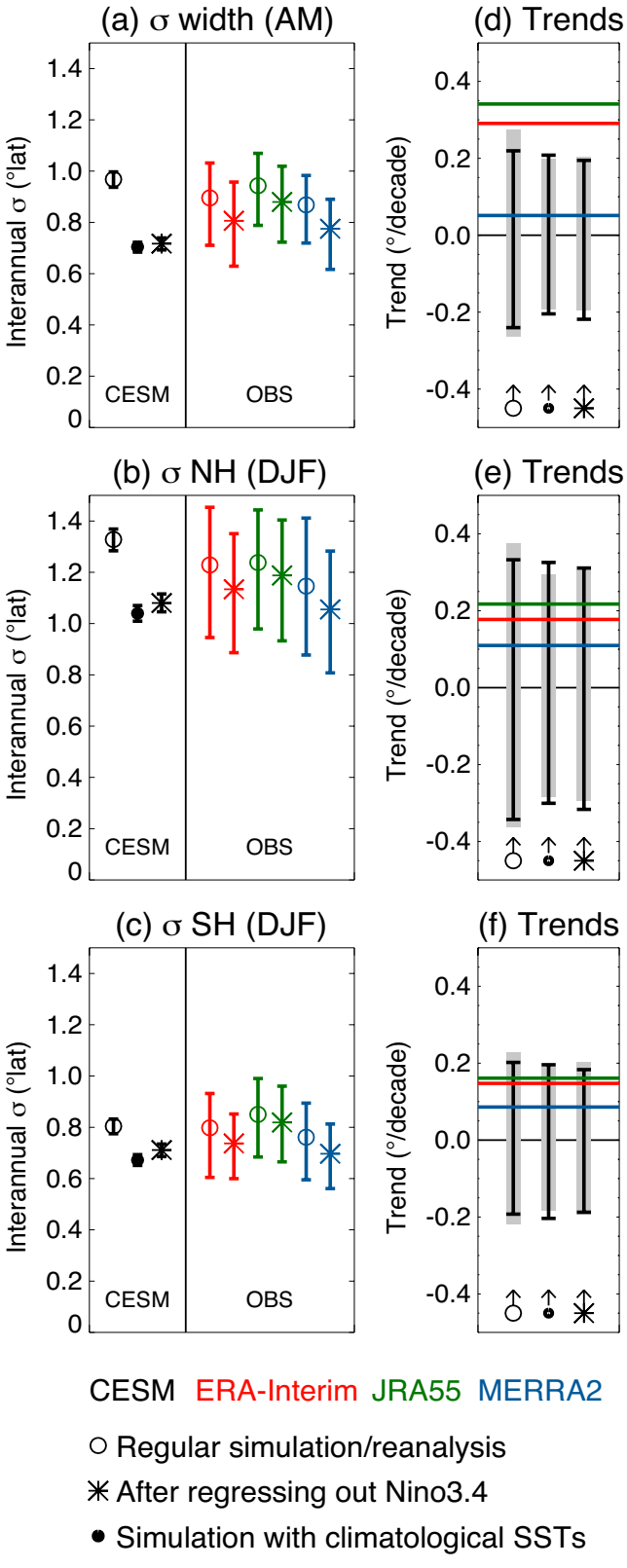

Figure 3. (a), (b) and (c) show interannual standard deviation of the annual mean tropical width, the DJF Northern Hemisphere tropical edge and the DJF Southern Hemisphere tropical edge respectively. CESM simulations and three reanalyses are shown. Open circles show the regular simulation/reanalysis; closed circle for CESM shows a simulation where the climatological SSTs of the coupled run are prescribed and asterisk shows the standard deviation after regressing out the contribution related to the Nino3.4 index (SST anomalies area averaged over 5°S–5°N, 190°E–240°E). The error bars depict the 2.5 to 97.5 percentile range of uncertainty on the value estimated using bootstrapping with replacement. (d), (e) and (f) show 38-year trends in annual mean tropical width, DJF Northern Hemisphere tropical edge and DJF Southern Hemisphere tropical edge, respectively. The grey bar shows the 2.5 to 97.5 percentile range of trends obtained from a synthetic white noise time series with the interannual standard deviation while the black bars show the actual 2.5 to 97.5 percentile range of 38-year trends from the simulations. The horizontal lines for reference show observed trends. The coupled piControl "regular" simulation with CESM is 1800 years long, and the simulation with climatological SSTs is 2600 years long.

Figure 3), indicating that the ocean's influence on tropical width occurs primarily through ENSO. Interannual variability is also reduced in the reanalyses upon regressing out the component related to ENSO, but the magnitude of this reduction is uncertain given the length of the records.

The 38-year trends that can arise as a result of internal atmospheric variability in CESM are almost as large as those found in the fully coupled simulation (Figure 3d,e). Based on CESM, internal atmospheric variability, which is inherently unpredictable, is capable of giving rise to trends over the length of the satellite record that are of the order 0.2° per decade for annual mean tropical width, 0.3° per decade for the Northern Hemisphere DJF edge, and 0.2° per decade for the Southern Hemisphere DJF edge. Given that CESM compares favorably with the reanalyses in terms of its interannual variability and no model gives any indication of long-term variability being more than the result of the random sampling of individual years, there is good reason to believe that this is also true of the real world; although this is difficult to conclude with certainty.

In summary, natural variability has likely played an important role in the trends that have been observed in tropical width in recent decades and will continue to influence the trends we observe in the future. A substantial fraction of this natural variability likely arises from internal atmospheric processes, with the remainder being accounted for primarily by ENSO variability. While we can make use of state-of-the-art global climate models to determine the magnitude of forced trends, we must continue to bear in mind the power of internal variability when it comes to isolating the influence of external forcings on our single observed record.

References

Adam, O., K. M. Grise, P. Staten, I. R. Simpson, S. M. Davis, N. A. Davis, D. W. Waugh, and T. Birner, 2018: The TropD software package: Standardized methods for calculating tropical width diagnostics. *Geosci. Mod. Dev*., submitted.

Allen, R. J., and M. Kovilakam, 2017: The role of natural climate variability in recent tropical expansion. *J. Climate*, **30**, 6329–6350, doi:10.1175/JCLI-D-16-0735.1.

Amaya, D. J., N. Siler, S.-P. Xie, and A. J. Miller, 2017: The interplay of internal and forced modes of Hadley Cell expansion: lessons from the global warming hiatus. *Climate Dyn*., doi:10.1007/s00382-017-3921-5.

Compo, G. P., and Coauthors, 2011: The Twentieth Century Reanalysis Project. *Quart. J. Roy. Met. Soc*., **137**, 1–28, doi:10.1002/qj.776.

Dee, D. P., and Coauthors, 2011: The ERA-Interim reanalysis: configuration and performance of the data assimilation system. *Quart. J. Roy. Met. Soc*., **137**, 553-597, doi:10.1002/qj.828.

DeWeaver, E., and S. Nigam, 1997: Dynamics of zonal-mean flow assimilation and implications for winter circulation anomalies. *J. Atmos. Sci*., **54**, 1758–1775, doi:10.1175/1520-0469(1997)054<1758:DOZMFA>2.0.CO;.

Davis, S. M., and K. H. Rosenlof, 2012: A multidiagnostic intercomparison of tropical-width time series using reanalyses and satellite observations. *J. Climate*, **25**, 1061–1078, doi:10.1175/JCLI-D-11-00127.1.

Frierson, D. M. W., J. Lu, and G. Chen, 2007: Width of the Hadley cell in simple and comprehensive general circulation models, *Geophys. Res. Lett.,* **34**, doi:10.1029/2007GL031115.

Garfinkel, C. I., D. W. Waugh, and L. M. Polvani, 2015: Recent Hadley cell expansion: The role of internal atmospheric variability in reconciling modeled and observed trends. *Geophys. Res. Lett*., **42**, 10824–10831, doi:10.1002/2015GL066942.

Gelaro, R. and Coauthors, 2017: The modern-era retrospective analysis for research and applications, version 2 (MERRA-2), *J. Climate*, **30**, 5419–5454, doi:10.1175/JCLI-D-16-0758.1.

Grassi, B., G. Redaelli, P. O. Canziani, and G. Visconti, 2012: Effects of the PDO phase on the tropical belt width. *J. Climate,* **25**, 3282–3290, doi:10.1175/JCLI-D-11-00244.1.

Kang, S. M., C., Deser, and L. M. Polvani, 2013: Uncertainty in climate change projections of the Hadley circulation: The role of internal variability. *J. Climate*, **26**, 7541–7554, doi:10.1175/JCLI-D-12-00788.1.

Kay, J. E., and Coauthors, 2015: The Community Earth System Model (CESM) Large Ensemble Project: A community resource for studying climate change in the presence of internal climate variability. *Bull. Amer. Meteor. Soc.,* **96**, 1333–1349, doi:10.1175/BAMS-D-13-00255.1.

Kidston, J., and E. P. Gerber, 2010: Intermodel variability of the poleward shift of the austral jet stream in the CMIP3 integrations linked to biases in 20th Century climatology. *Geophys. Res. Lett*., **37**, doi:10.1029/2010GL042873.

Kobayash, S., and Coauthors, 2015: The JRA-55 Reanalysis: General specifications and basic characteristics. *J. Meteor. Soc. Japan*., **93**, 5-48, doi:10.2151/jmsj.2015-001.

Lucas, C., B. Timbal, and H. Nguyen, 2014: The expanding tropics: a critical assessment of the observational and modeling studies. *WIREs Climate Change*, **5**, 89-112, doi:10.1002/wcc.251.

Lu, J., G. A. Vecchi, and T. Reichler, 2007: Expansion of the Hadley cell under global warming. *Geophys. Res. Lett.,* **34**, doi:10.1029/2006GL028443.

McLandress, C., T. G. Shepherd, J. F. Scinocca, D. A. Plummer, M. Sigmond, A. I. Jonsson, M. C. Reader, 2011: Separating the dynamical effects of climate change and ozone depletion. Part 2: Southern Hemisphere troposphere. *J. Climate,* **24**, 1850–1868, doi:10.1175/2010JCLI3958.1.

Mantsis, D. F., S, Sherwood, R. Allen, and L. Shi, 2016: Natural variations of tropical width and recent trends. *Geophys. Res. Lett*., **44**, 3825–3832, doi:10.1002/2016GL072097.

Nguyen, H., A. Evans, C. Lucas, I. Smith, and B. Timbal, 2013: The Hadley Circulation in reanalyses: Climatology, variability, and change. *J. Climate,* **26**, 3357–3376, doi:10.1175/JCLI-D-12-00224.1.

Polvani, L. M., D. W. Waugh, G. J. P. Correa, S.-W. Son, 2011: Stratospheric ozone depletion; the main driver of 20th Century atmospheric circulation changes in the Southern Hemisphere, *J. Climate*, **24**, 795–812, doi:10.1175/2010JCLI3772.1.

Poli, P., and Coauthors, 2016: ERA-20C: An atmospheric reanalysis of the Twentieth Century. *J. Climate*, **29**, 4083–4097, doi:10.1175/JCLI-D-15-0556.1.

Quan, X.-W., M. P. Hoerling, J. Perlwitz, H. F. Diaz, and T. Xi, 2014: How fast are the tropics expanding? *J. Climate*, **27**, 1999–2013, doi:10.1175/JCLI-D-13-00287.1.

Quan, X.-W., M. P. Hoerling, J. Perlwitz, and H. F. Diaz, 2018: On the time of emergence of tropical width change. *J. Climate,* submitted.

Seidel, D. J, Q. Fu, W. J., Randel, and T. J. Richler, 2008: Widening of the tropical belt in a changing climate. *Nat. Geosci,* **1**, 21–24, doi:10.1038/ngeo.2007.38.

Simpson, I. R., and L. M. Polvani, 2016: Revisiting the relationship between jet position, forced respons, and annular mode variability in the southern midlatitudes. *Geophys. Res. Lett.,* **42**, 2896–2903, doi:10.1002/2016GL067989.

Solomon, A., and L. M. Polvani, 2016: Highly significant responses of anthropogenic forcings of the midlatitude jet in the Southern Hemisphere. *J. Climate,* **29**, 3462–3470, doi:10.1175/JCLI-D-16-0034.1.

Tao, L, Y. Hu, and J. Liu, 2016: Anthropogenic forcing of the Hadley circulation in CMIP5 simulations. *Climate Dyn*., **46**, 3337–3350, doi:10.1007/s00382-015-2772-1.

Waugh, D. W., C. I. Garfinkel, and L. M. Polvani, 2015: Drivers of the recent tropical expansion in the Southern Hemisphere: Changing SSTs or ozone depletion? *J. Climate,* **28**, 6581–6586, doi:10.1175/JCLI-D-15-0138.1.

Waugh, D. W., and Coauthors, 2018: Revisiting the relationship among metrics of tropical expansion. *J. Climate*, submitted.

Poleward expansion only dries subtropical land in certain, specific regions and seasons

Jacob Scheff

University of North Carolina, Charlotte

The climatology of precipitation on Earth is broadly characterized by a wet tropical belt associated with the rising branch of the Hadley cell, wet mid-latitude belts associated with the northern and southern baroclinic storm tracks, and the dry subtropical belts between that are associated with the descending branches of the Hadley cell.

About a decade ago, researchers noticed that according to multiple zonal-mean metrics, the general circulation seemed to be expanding poleward in subtropical to mid-latitudes (e.g., Seidel et al. 2008 and references therein) and that climate models robustly project this expansion to continue in response to global warming (e.g., Yin 2005; Lu et al. 2007). Critically, this literature expressed concern that reductions in water supplies on the poleward margins of the subtropics would result, as mid-latitude wetness would be replaced by subtropical dryness. More recent observational studies using modern reanalyses and objective metrics (e.g., Birner 2010; Rikus 2015; Davis and Birner 2017) have broadly confirmed these zonal-mean results, though with reduced magnitude and/or lower confidence, particularly in the Northern Hemisphere.

Yet, no one lives in the zonal mean: the full 2D structure of climatological precipitation is actually quite complicated due to monsoons, topography, and the oceanic subtropical gyres (e.g., Hartmann 2016). This is particularly true in the summer, when several large and strong wet belts diagonally bridge the subtropics, linking the tropical and mid-latitude wet zones together (e.g., Scheff and Frierson 2012a). Also, the projected wintertime storm-track changes are very zonally asymmetric. Thus, it is unclear exactly which places would expect to see precipitation declines from the zonal-mean poleward expansion of the subtropics.

In particular, precipitation decline over *land* is much more consequential for society than precipitation decline over the ocean, because only land-based precipitation creates freshwater resources for human use and because only land-dwelling plants need to be watered. Yet land makes up only a minority of the subtropical surface. Studies such as Seager et al. (2010), Scheff and Frierson (2012a,b), and He and Soden (2016) confirmed that precipitation and precipitation-minus-evaporation are projected to decline across broad regions of the subtropical-to-mid-latitude transition in 2D (not just in the zonal mean), and that these declines are indeed caused by circulation change. However, they did not specifically focus on land, leading them to conclusions that mainly hold over the ocean and are, thus, largely irrelevant to society.

In fact, He and Soden (2016) found that the ocean- and land-based drying are caused by fundamentally different mechanisms. Ocean-based drying is largely a direct consequence of the rise in CO_2 itself, via "fast" ocean-to-land zonal circulation responses. Only the land-based drying (which is quite spatially confined) is significantly

caused by planetary warming and the attendant meridional circulation expansion. Thus, we would not expect them to be similar.

Indeed, Schmidt and Grise (2017) showed that in year-to-year variability, land precipitation is only sensitive to the zonal-mean Hadley cell edge latitude in certain specific subtropical regions. That is, most of Earth's subtropical land precipitation is not at all sensitive to Hadley cell width variations as usually measured. So we might expect that the projected expansion of the subtropical dry zones and Hadley cells with global warming will only cause land precipitation to decline in certain, specific regions.

Here, I examine the Scheff and Frierson (2012b) results on robust CMIP5-projected subtropical precipitation declines but with an explicit focus on land precipitation. The broad conclusions of that study about Hadley-driven poleward expansion of subtropical dryness are much less relevant over most of the land than over the ocean. The projections of land-based drying are far less widespread and far less uniformly poleward-expansion driven than implied by that largely ocean-based study.

Interpretation of CMIP5 projections of drying over land

Figure 1 is a reproduction from Scheff and Frierson (2012b). The four maps correspond to the four meteorological seasons (December-February, March-May, June-August, and September-November). On each map, the continents are outlined in cyan. The black curves are contours of climatological seasonal-mean precipitation as simulated by the CMIP5 36-model average. The lightest contour (1 mm/day) encircles the hearts of the subtropical dry zones, the intermediate contour (2 mm/day) broadly separates the dry and wet zones, and the boldest contour (5 mm/day) encircles the tropical wet belt and the wettest parts of the mid-latitude wet belts.

According to the triangular legend at the top, locations where most of the 36 models project precipitation to *significantly decline* with strong global warming (RCP8.5 scenario) are colored in bold red, locations where most models project precipitation to significantly increase are colored in bold blue, and locations where most models project insignificant precipitation changes are colored in white or very light colors. Intermediate intensity and/or purple hues correspond to regions of inter-model disagreement, which are extensive.

In each season, the continents can be carefully examined for regions of robustly projected significant drying (bold red color), which can then be compared to the black climatology contours to assess whether they are likely to be related to poleward expansion of the dry zones.

In December-February (northern winter/southern summer, Figure 1a), land drying is clearly projected in coastal portions of North Africa, the Middle East, and southern Europe in the Mediterranean Basin. This is right on the edge between the Saharan dry zone and the European storm track, so it clearly represents classic subtropical expansion drying. Similarly in Chile, the region between the central drylands and the southern temperate rainforest, where the subtropical flank of the Pacific storm track reaches the continent around 40°S, is projected to dry.

However, these are the only such regions on the planet: no other land areas in the entire Southern Hemisphere are colored bold red in December-February. The other robust southern drying regions, highlighted in Scheff and Frierson (2012b), are simply too far south to affect Australia or Africa. In the Northern Hemisphere, the north coast of South America is projected to dry, but this is located on the equatorward edge of the subtropical dry zone, so it could not be associated with poleward expansion of the circulation.

A region from Mexico into the far southwestern US is also projected to dry in December-February, but this coincides with a spurious feature of the multi-model precipitation climatology that is not present in reality: a wet belt extending meridionally from the East Pacific

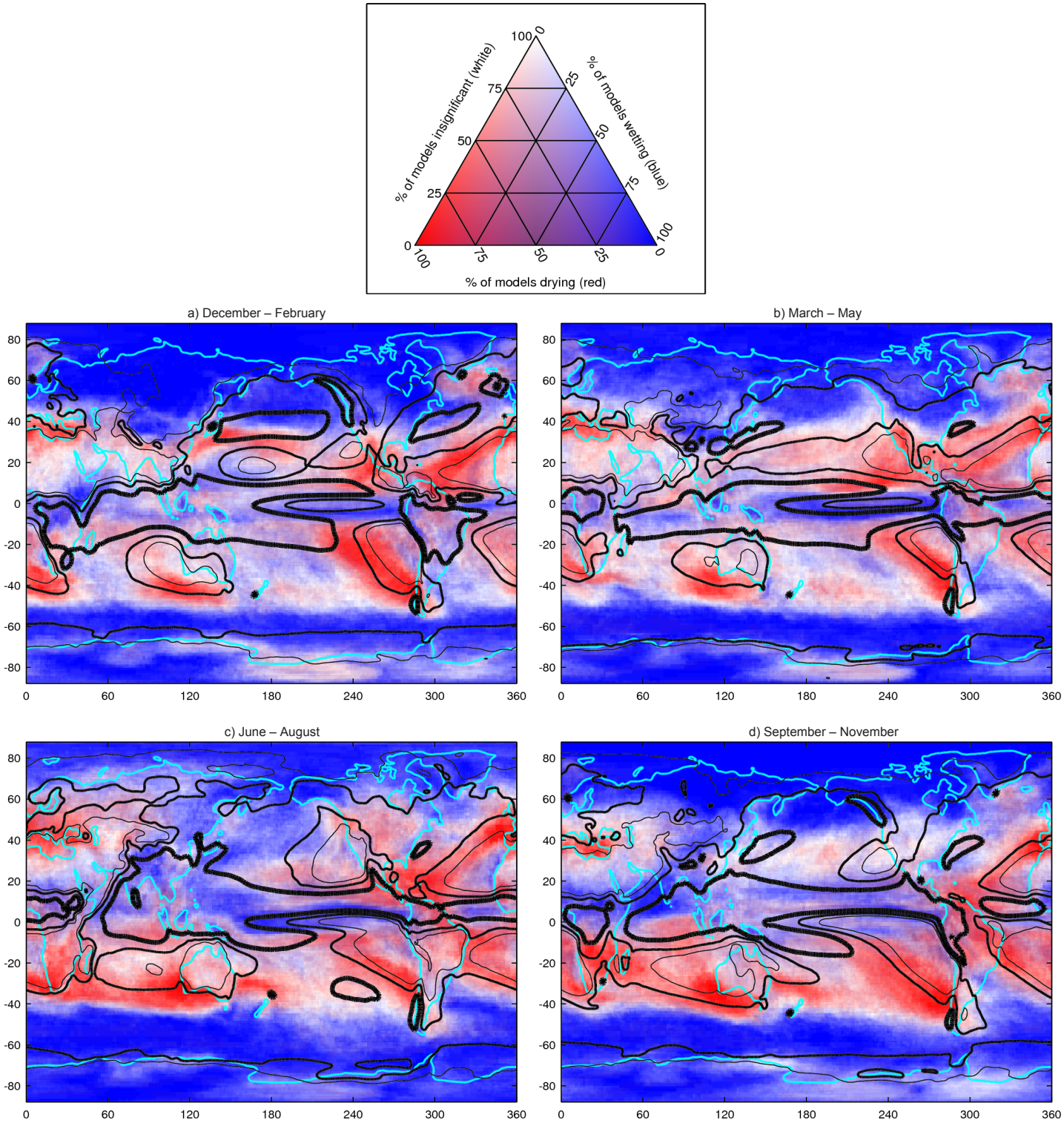

Figure 1. In each season, black contours are the 1980–1999 CMIP5 multi-model climatological precipitation (1, 2, 5 mm/day, going from lightest to boldest). At each point, the colored shading shows the proportion of CMIP5 models for which the RCP8.5 1980–2099 seasonal precipitation trend in the native model gridbox containing that point is negative and significant (red), positive and significant (blue), or insignificant (white), according to the legend. Significance level is 5%.

Intertropical Convergence Zone (ITCZ) across much of Mexico to the beginning of the Atlantic storm track over the northern Gulf of Mexico coast. In actuality, this region receives extremely little precipitation in winter (generally less than 0.3 mm per day, as opposed to the substantial >2 mm per day simulated by the models). So the models are projecting the drying of a feature that does not really exist. In contrast, there is no robust drying projected at the poleward edges of the two nearby subtropical dry zones in California and Central America.

In March-May (northern spring/southern autumn; Figure 1b), the Mediterranean and Chilean poleward-expansion drying regions are still very apparent, and both are shifted somewhat north relative to December-February. Another small but clear poleward-expansion land drying region appears in parts of the western US and far northwest Mexico (well to the northwest of the spurious December-February drying), at the northern apex of the Pacific subtropical dry zone, or southern flank of the western US storm track. However, those are the only substantial robust land-based drying regions on Earth projected for March-May. The vast majority of subtropical land is not robustly projected to dry in this season, by any mechanism. There is a hint that robust drying may extend to the extreme southwest tips of Africa and Australia in this season, but it is not clear.

In June-August (northern summer/southern winter, Figure 1c), there are more regions of projected land drying. The Mediterranean poleward-expansion drying now encompasses much of the European continent, as southern European summer dryness replaces northern European wetness. The Chilean poleward-expansion drying is also still strong. The western North American drying is no longer present, but the South Atlantic and South Indian Ocean poleward-expansion drying belts now finally intersect southwestern Africa (the Cape region) and southwestern Australia in a substantial way.

Drying is also robustly projected well into the interior of southern Africa, but again this region receives essentially no winter rainfall (in the models or in reality), so it is inconsequential. Drying is projected across much of Central America and (less robustly) in the far-western Sahel and northeastern South America, but these are again located on the equatorward edges of the dry zones rather than the poleward edges, so could not be caused by poleward circulation expansion.

Finally, in September-November (northern autumn/southern spring; Figure 1d), a couple of interesting new projected land-drying regions emerge. The classic Mediterranean, Chilean, far south/southwest Australian, and Cape African poleward-expansion-driven areas are still apparent. However, there is also very robust drying projected in the interior of southern Africa around 10-25°S (which now receives substantial rain, unlike in winter) and somewhat robust drying projected in tropical northeast Brazil.

Both of these latter responses might also possibly be caused by poleward expansion of the circulation: the southern African drying is located at a "saddle" in the precipitation field where mid-latitude precipitation reaches equatorward, and the northeast Brazilian drying is located on the poleward/westward side of the South Atlantic dry zone, where it grades into the wet South Atlantic Convergence Zone. However, they are both located in tropical latitudes and substantially affect tropical rather than mid-latitude precipitation, so it is not clear whether poleward expansion of the Hadley cell edge could physically cause them.

Synthesis and discussion

Robustly projected reductions in *land* precipitation that are likely caused by the *poleward expansion of the atmosphere's general circulation* are confined to very specific regions (and often very specific seasons). These consist of the Mediterranean/European area and Chile all-year round (further poleward in the local warm season and further equatorward in the local cool season); a modest portion of interior western North America in local spring only; extreme southwestern Africa (the Cape

region) and extreme southwestern/southern Australia in local winter, spring, and possibly fall; and possibly interior southern Africa and northeast Brazil in local spring. Many (but not all) of these are located in Mediterranean, winter-rain climate zones, as one might expect. Many also correspond to the specific regions highlighted by Schmidt and Grise (2017) where the zonal-mean Hadley cell's edge latitude is strongly correlated with local land precipitation in year-to-year variability and to the specific regions found by He and Soden (2016) where subtropical drying is caused by warming, rather than by direct CO_2 effects.

Other regions/seasons of robustly projected subtropical land drying are clearly unrelated to poleward expansion (e.g., Central America in local summer) and/or are likely spurious (e.g., Mexico and vicinity in local winter). In fact, Figure 1 shows that the vast majority of subtropical land is *not* robustly projected to be affected by poleward-expansion related drying: the North American subtropics outside of the specific area mentioned above, the South American subtropics east of the Andes, the vast African and Australian subtropical belts outside of the small coastal zones highlighted above (with the possible exception of interior southern Africa in spring), and the entire Asian subtropics. This was noted to some degree in Scheff and Frierson (2012b) but not explicitly. This also parallels the conclusion from Schmidt and Grise (2017) that precipitation over most subtropical land gridpoints is not at all correlated with the zonal-mean Hadley cell edge latitude. Over land, projections for precipitation-minus-evaporation are broadly similar to precipitation projections but weaker and much less robust (Scheff et al. 2017), so using precipitation-minus-evaporation instead of precipitation would not be likely to yield additional robust drying areas.

Why does the poleward expansion of the circulation with warming fail to broadly and robustly dry subtropical land in CMIP5 projections? The most basic reason may be that the fully 2D subtropical dry zones are preferentially located over the oceans (black contours in Figure 1), so that their poleward expansion disproportionately affects precipitation over oceans. Indeed, most of the land poleward-expansion drying regions listed above are simply downstream (eastward) continuations of much larger poleward-expansion drying regions over the ocean.

However, Figure 1 also shows that there are still vast regions over land that are clearly in the transition belts between subtropical dry zones and mid-latitude wet zones yet are not robustly projected to become drier with global warming. These include (among other regions) the American West in seasons other than springtime, most of southern Australia, much of subtropical South America, and almost all of Central Asia. Many of the subtropical-to-mid-latitude transition belts over the ocean do not robustly dry with warming either, such as in the North Pacific for most of the year. Thus, the lack of poleward-expansion drying over much of land is also simply because a zonal-mean subtropical expansion or zonal-mean storm-track shift does not imply that these features move poleward at *every* longitude but just at some. In addition, He and Soden (2016) found that the direct effect of CO_2 increase is to reduce precipitation over parts of the subtropical oceans but *increase* precipitation over parts of the subtropical land, offsetting part of the poleward-expansion induced drying that might otherwise be expected on land.

In conclusion, despite earlier studies tacitly implying that the poleward expansion of the general circulation would cause a broad reduction in water supplies on the poleward edges of the subtropical dry zones, such projections are actually quite spatially and seasonally confined in multi-model CMIP5 output over land. This discrepancy arises from key climatological and climate-response differences between the land (where precipitation matters to society) and the ocean (where most of the earlier 2D studies were effectively focused), as well as from the basic fact that a zonal-mean response does not imply a similar response at each longitude or even at most longitudes. Future work should seek to better understand this zonal asymmetry by uncovering the key dynamical mechanisms for tropical expansion and the ways that those mechanisms are expressed in latitude-longitude space, neither of which is well understood today.

References

Birner, T., 2010: Recent widening of the tropical belt from global tropopause statistics: sensitivities. *J. Geophys. Res.*, **115**, doi:10.1029/2010JD014664.

Davis, N., and T. Birner, 2017: On the discrepancies in tropical belt expansion between reanalyses and climate models and among tropical belt width metrics. *J. Climate*, **30**, 1211–1231, doi:10.1175/JCLI-D-16-0371.1.

Hartmann, D., 2016: *Global Physical Climatology*, 2nd Ed. Elsevier, 498 pp, ISBN: 9780080918624.

He, J., and B. J. Soden, 2016: A re-examination of the projected subtropical precipitation decline. *Nature Climate Change*, **7**, 53–57, doi:10.1038/nclimate3157.

Lu, J., G. A. Vecchi, and T. J. Reichler, 2007: Expansion of the Hadley cell under global warming. *Geophys. Res. Lett.*, **34**, doi:10.1029/2006GL028443.

Rikus, L., 2015: A simple climatology of westerly jet streams in global reanalysis datasets part 1: mid-latitude upper tropospheric jets. *Climate Dyn.*, **50**, 2285–2310, doi:10.1007/s00382-015-2560-y.

Scheff, J., and D. Frierson, 2012a: Twenty-first-century multimodel subtropical precipitation declines are mostly midlatitude shifts. *J. Climate*, **25**, 4330–4347, doi:10.1175/JCLI-D-11-00393.1.

Scheff, J., and D. M. W. Frierson, 2012b: Robust future precipitation declines in CMIP5 largely reflect the poleward expansion of model subtropical dry zones. *Geophys. Res. Lett.*, **39**, doi:10.1029/2012GL052910.

Scheff, J., R. Seager, H. Liu, and S. Coats, 2017: Are glacials dry? Consequences for paleoclimatology and for greenhouse warming. *J. Climate,* **30**, 6593–6609, doi:10.1175/JCLI-D-16-0854.1.

Schmidt, D. F., and K. M. Grise, 2017: The response of local precipitation and sea level pressure to Hadley cell expansion. *Geophys. Res. Lett.*, **44**, 10573–10582, doi:10.1002/2017GL075380.

Seager, R., N. Naik, and G. A. Vecchi, 2010: Thermodynamic and dynamic mechanisms for large-scale changes in the hydrological cycle in response to global warming. *J. Climate*, **23**, 4651–4668, doi:10.1175/2010JCLI3655.1.

Seidel, D. J., Q. Fu, W. J. Randel, and T. J. Reichler, 2008: Widening of the tropical belt in a changing climate. *Nature Geosci.*, **1**, 21–24, doi:10.1038/ngeo.2007.38.

Yin, J., 2005: A consistent poleward shift of the storm tracks in simulations of 21st century climate. *Geophys. Res. Lett.*, **32**, doi:10.1029/2005GL023684.

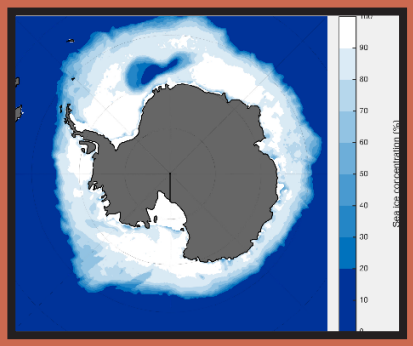

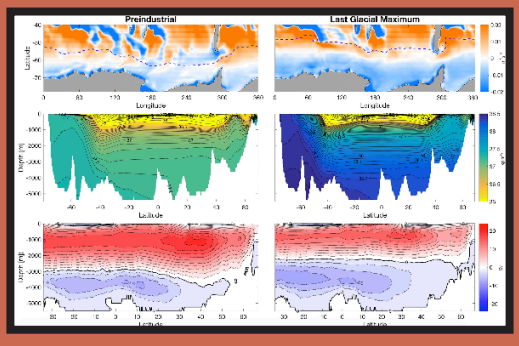

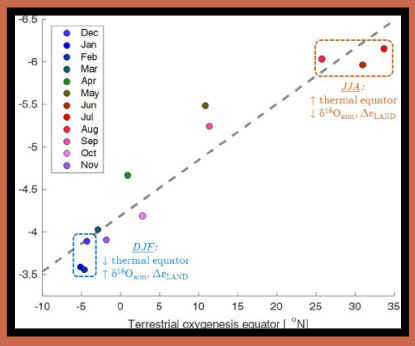

Expanding width of the tropics: Impacts on the ocean

Kerry H. Cook and Edward K. Vizy

The University of Texas at Austin

Atmosphere and ocean coupling through the exchange of water, energy, and momentum suggests that shifts in the position (and intensity) of the Hadley circulation will hold implications for the oceans. Of primary concern are changes induced in the ocean mixed layer, including currents and upwelling, and their potential impacts on marine ecosystems and fisheries.

Subtropical highs and ocean gyres

One way that an expansion of the tropics may have repercussions for the oceans is through the intensity and positioning of the subtropical highs over the ocean basins. Wind stress exerted on the ocean surface by anticyclonic flow around the subtropical highs, combined with the physical east/west boundaries of the ocean basins, organizes ocean currents into gyres (Figure 1). There are additional influences on the subtropical highs in addition to the Hadley circulation, including regional circulations such as monsoons and decadal-scale modes of variability, but an expansion of the tropics can be expected to shift the subtropical highs poleward.

Figure 2 shows annual mean sea level pressure trends over the 1980–2017 time period from three second-generation atmospheric reanalyses. These trends are in good agreement among the reanalyses, and indicate an intensification and a northwestward (southwestward) shift of the subtropical anticyclone over the North (South) Pacific, a weaker westward shift of the North Atlantic subtropical high (NASH), a distinct southward shift of the South Atlantic subtropical high (SASH), and a southeastward shift of the South Indian Ocean Mascarene high. These changes in the subtropical anticyclones are generally significant at the 90% level of confidence for the Pacific and South Atlantic basin but not for the North Atlantic and South Indian Oceans.

Regional and seasonal studies are consistent with the trends shown in Figure 2. Li et al. (2011) observed that

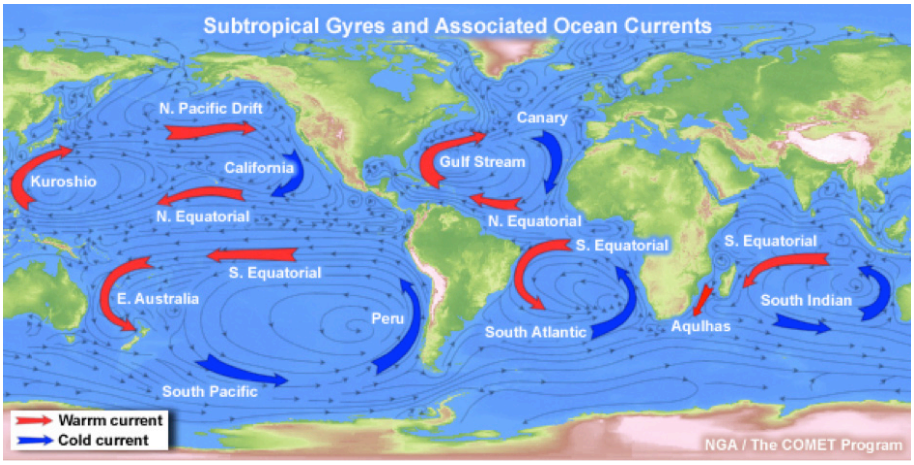

Figure 1. Ocean currents and their configuration as subtropical gyres.

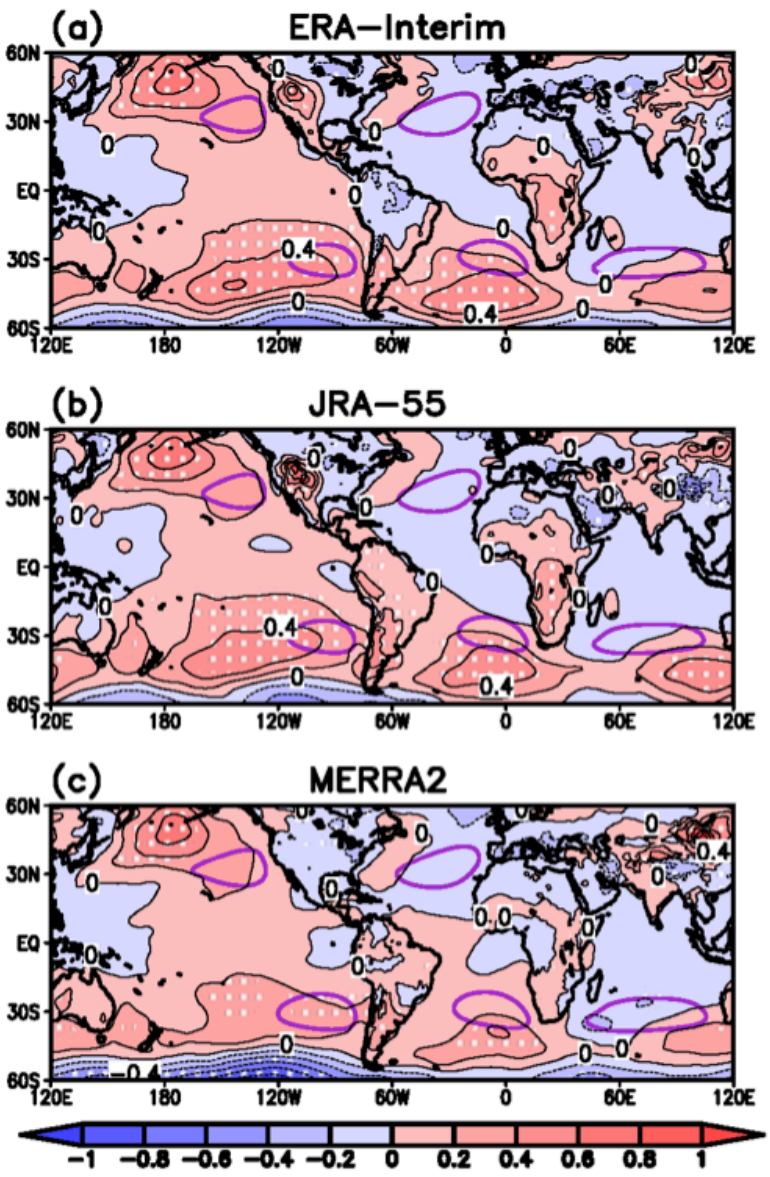

Figure 2. 1980–2017 annual mean sea level pressure trends (shaded; hPa per decade) for (a) ERA-Interim, (b) JRA-55, and (c) MERRA2 reanalyses. Purple contours indicate the climatological positions of the sub-tropical anticyclones over the ocean basins as inferred from the 1020 hPa contours. Stippling denotes values found statistically significant at the 90% level of confidence after taking into account autocorrelation using the Zwiers and von Storch (1995) two-stage table lookup test procedure.

the NASH has been shifting westward during the summer months. Similarly, Lu and Dong (2001), Sui et al. (2007), and Zhou et al. (2009) note a westward shift and intensification of the North Pacific anticyclone during the boreal summer. The changes in the North Pacific have been attributed to an increase in the thermal contrast between the oceans and the adjacent continents, combined with Indian Ocean and western Pacific warming trends (Zhou et al. 2009; Li et al. 2012). A poleward shift of the Northern Hemisphere subtropical anticyclones may be more difficult to discern in the trend patterns due in part to the greater presence of land compared with the Southern Hemisphere.

The South Atlantic provides a good region for examining shifts in the subtropical high. The subtropical high is well formed in this basin, and a poleward shift of the SASH is distinct in the annual mean (Figure 2). Vizy et al. (2018) quantify annual mean changes in the SASH since 1980. There has been a significant increase in intensity of +0.12 to +0.24 hPa per decade. This intensification is accompanied by a poleward shift of -0.22 to -0.34° latitude per decade, and a westward shift of -0.05 to -0.20° longitude per decade in the SASH's central position. This shift is expected to continue through the century, as shown in the regional model projections for the mid- and late-21st century in Figure 3.

The South Atlantic Ocean is adjusting to these trends in the SASH. For example, the Angola-Benguela frontal zone (ABFZ) in the eastern subtropical South Atlantic Ocean, where cold equatorward-flowing waters associated with the Benguela Current converge with the poleward-flowing warm waters of the Angola Current, has been changing along with the atmospheric circulation. The ABFZ has been shifting poleward by 0.05 to 0.55° per latitude decade and intensifying in strength by 0.05 to

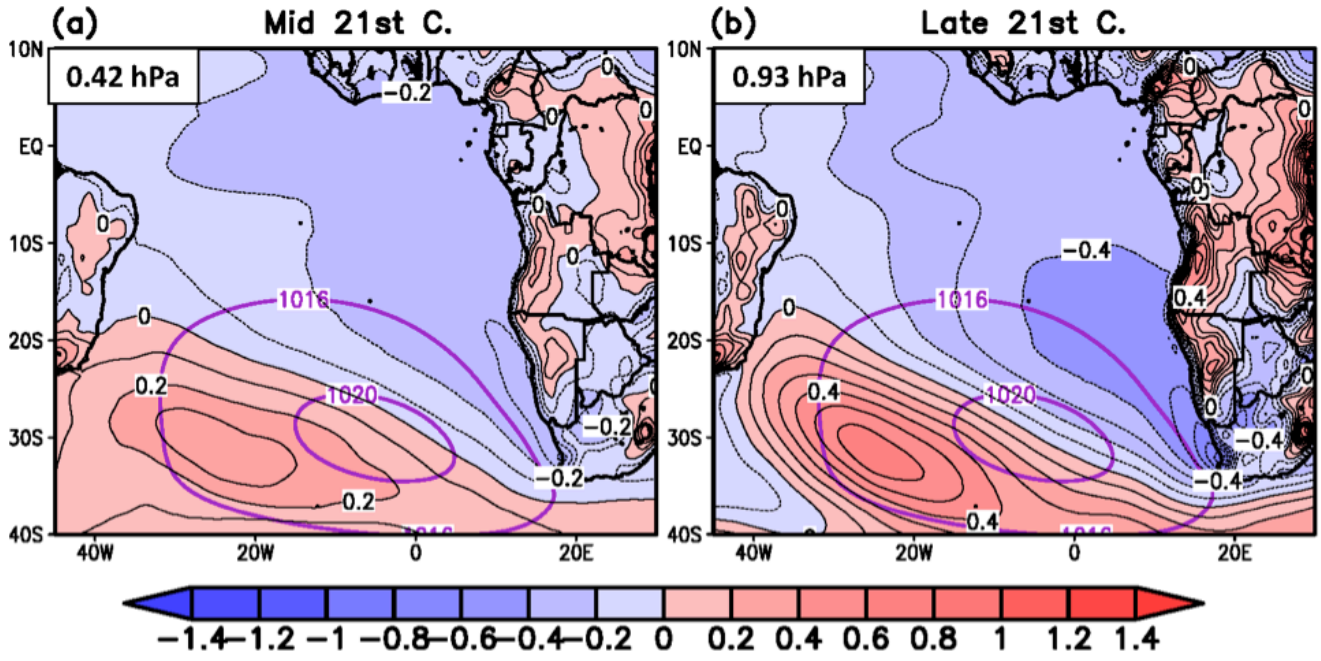

Figure 3. Projected November–January weighted mean sea level pressure anomalies (hPa) for (a) mid-21st century (2041–2060), and (b) late-21st century (2081–2100) from 90 km regional climate model time-slice simulations of Vizy et al. (2013). The value of the domain-averaged anomaly subtracted from each period to weight the anomaly field is provided in each panel. The late-20th century location of the SASH is denoted by the 1016 and 1020 hPa purple contours in each panel.

0.13 K/100 km per decade since 1980 (Vizy et al. 2018). The warming to the north of the ABFZ is associated with reduced onshore low-level flow, while cooling to the south of the ABFZ is related to an enhanced equatorward transport of cooler water from mid-latitudes associated with stronger surface winds over the Benguela upwelling region. Both responses are consistent with a poleward shift of the SASH.

Seasonality may also be an important factor when trying to understand changes in the Mascarene high over the South Indian Ocean. Vizy and Cook (2016) analyze mean sea level pressure trends for the three month period of November–January and find that the Mascarene high has undergone a poleward shift during this period rather than southeastward as indicated in the annual mean (Figure 2). However, these trends are not highly significant and additional investigation is needed.

Eastern boundary currents and upwelling

Eastern boundary currents (EBCs), denoted by the equatorward blue arrows in Figure 1, are cool ocean currents located along the eastern flanks of the oceanic subtropical highs, beneath equatorward climatological flow. There are four major EBCs on the planet: the Canary Current in the North Atlantic, the California Current in the North Pacific, the Benguela Current in the South Atlantic, and the Peru (or Humboldt) Current in the South Pacific. Coriolis accelerations acting on this nominally equatorward flow at the surface create a westward net mass flux in the ocean Ekman layer in both hemispheres. The westward water mass flux associated with the EBCs transports mass away from the west coasts of the continents, triggering coastal upwelling. This upwelling reinforces cool temperatures in the eastern subtropical ocean basins, feeding back to atmospheric circulation

features such as the subtropical highs and modifying land/sea temperature contrasts.

In additional to effects from shifts in the Hadley circulation as delivered through the subtropical highs, trends in land/sea temperature contrasts can influence EBCs and upwelling (Bakun et al. 1990). Wang et al. (2015) found that coupled general circulation models (GCMs) produce a strong, positive correlation between the intensity of upwelling and the magnitude of the land/sea temperature contrast in the summer for all EBCs except the California Current. The physical processes responsible for this connection were not explored and could be related to local wind changes such as land/sea breeze and monsoon circulations. In addition, changes in ocean stratification must be considered in any climate change scenario, as surface warming stabilizes the water column. Nonetheless, a poleward shift of the subtropical highs may also be involved, especially since the correlation was most robust at higher latitudes.

Observations of upwelling trends in the 20th and early 21st centuries are reported regionally. Gutierrez et al. (2011) examined observed SSTs and reconstructed SSTs from a sediment core located in the main upwelling region off the coast of Peru over the last 150 years. A comparison with reanalysis winds related cooling SSTs, indicative of stronger upwelling, with intensified alongshore winds. Schneider et al. (2017) reported pronounced increases in winds favorable for upwelling off the central-south Chilean coast are accompanied by strong, cooling waters, indicative of intensified upwelling over the 2002–2013 time period. They related these changes to a southward displacement of the South Pacific subtropical high since 2007.

Garcia-Reyes and Langler (2010) reported increases in wind-driven upwelling from 1982–2008 along a 400 km stretch of the central California coast (35ºN–39ºN) but did not find significant trends to the north and south of this region. For the Benguela upwelling off the Namibian coast, Santos et al. (2012) observed an intensification of coastal upwelling that was consistent with observed changes in the position and intensity of the South Atlantic high and suggested a connection with the Southern Annular Mode.

Oerder et al. (2015) used a regional ocean model driven by surface winds from a GCM to study CO_2-induced changes in the Peru Current and its implications for coastal upwelling. They did not report a shift in the upwelling, which could accompany a widening of the tropics (all other conditions being unchanged), but a weakening of the upwelling in association with weakened along-shore wind stress and wind stress curl. Garreaud and Falvey (2009) and Belmadani et al. (2014) suggest that the coastal topography of South America may play a role in Peru Current trends, weakening or interrupting large-scale interactions. A recent modeling study of the Canary upwelling system revealed pronounced seasonality in the projections, with weakened upwelling in May through August and strengthened upwelling from October through April (Sousa et al. 2017).

Rykaczewski et al. (2015) examined output from 21 CMIP5 GCMs, comparing a preindustrial period (1861–1890) from historical simulations with an end-of-century period (2071–2100) forcing with the RCP8.5 emissions scenario. They investigated changes in upwelling regions, including any relationship to trends in land/sea temperature contrast. While land/sea temperature contrasts increase throughout the 21st century in the models, they are not accompanied by intensification of upwelling in the California, Canary, Benguela, and Peru EBC systems, which is consistent with the GCM-based results of Mote and Mantua (2002). The breakdown in the connection between increased land/sea temperature contrast and intensified upwelling occurs in the first step, when land surface warming is not uniformly accompanied by a deepening of continental thermal lows (similar to the results of Hsieh and Boer 1992). However, a robust response does emerge from the multi-model ensemble when upwelling (measured as a surface wind stress favorable for upwelling) intensifies in the poleward portions of the four upwelling regions and weakens in the equatorward portions.

Concluding remarks

Observational and modeling studies provide crucial information about ongoing and potential changes in ocean currents, including upwelling, in association with an expansion of the tropics, but more research is needed to establish robust greenhouse gas-induced trends and projections. Of special concern are coastal upwelling regions, which supply about 20% of the global fish catch. Coupled with physical responses to tropical widening in the ocean system, which exhibit regional and seasonal variations, is the need to understand biological responses. The ecosystem response will likely be complicated and species dependent, and also highly regional and seasonal. For example, Xiu et al. (2018) simulated an intensification of upwelling off the coast of California, but in their model the response of the plankton community to an increase in nutrients was complicated due to the complex and nonlinear food web dynamics. Changes in upwelling not only modify the delivery of nutrients to surface waters but also perturb ocean chemistry. For example, upwelling water is relatively depleted in oxygen and can enlarge regions of hypoxia (Grantham et al. 2004).

It is clear that ocean current and coastal upwelling systems are not static. They are sensitive to changes in the position of the subtropical highs to the west of the EBCs and land/sea contrasts. These sensitivities suggest that the global oceans will respond to an expansion of the tropics and will potentially feedback to the atmosphere to modify the expansion. This research should be pursued with high priority.

References

Bakun, A., 1990: Global climate change and intensification of coastal ocean upwelling. *Science,* **247**, 198–201, doi:10.1126/science.247.4939.198.

Belmadani, A., V. Echevin, F. Codron, K. Takahashi, and C. Junquas, 2014: What dynamics drive future wind scenarios for coastal upwelling off Peru and Chile? *Climate Dyn.,* **43**, 1893–1914, doi:10.1007/s00382-013-2015-2.

Garcıa-Reyes, M. and J. Largier, 2010: Observations of increased wind-driven coastal upwelling off central California. *J. Geophys. Res*. **115**, doi:10.1029/2009JC005576.

Garreaud, R. D., and M. Falvey, 2009: The coastal winds off western subtropical South America in future climate scenarios. *Int. J. Climatol*., **29**, 543–554, doi:10.1002/joc.1716.

Grantham, B. A., F. Chan, K. J. Nielsen, D. S. Fox, J. A. Barth, A. Huyer, J. Lubchenco, and B. A. Menge, 2004: Upwelling-driven nearshore hypoxia signals ecosystem and oceanographic changes in the northeast Pacific. *Nature*, **429**, 749–754, doi:10.1038/nature02605.

Gutierrez, D., and Coauthors, 2011: Coastal cooling and increased productivity in the main upwelling zone off Peru since the mid-twentieth century. *Geophys. Res. Lett.,* **38,** doi:10.1029/2010GL046324.

Hsieh, W. W., and G. J. Boer, 1992: Global climate change and upwelling. *Fish Oceanogr*., **1**, 333–338, doi:10.1111/j.1365-2419.1992.tb00005.x.

Li, W., L. Li, R. Fu, Y. Deng, and H. Wang, 2011: Changes to the North Atlantic subtropical high and its role in the intensification of summer rainfall variability in the Southeastern United States. *J. Climate*, **24**, 1499–1506, doi:10.1175/2010JCLI3829.1.

Li, W., L. Li, M. Ting, and Y. Liu, 2012: Intensification of Northern Hemisphere subtropical highs in a warming climate. *Nat. Geosci.*, **5**, 830–834, doi:10.1038/NGEO1590.

Lu, R., and B. Dong, 2001: Westward extension of North Pacific subtropical high in summer. *J. Meteorol. Soc. Jap. Ser. II,* **79,** 1229–1241, doi:10.2151/jmsj.79.1229.

Mote, P. W., and N. J. Mantua, 2002: Coastal upwelling in a warmer future. *Geophys. Res. Lett*. **29**, 53-1–53-4, doi:10.1029/2002GL016086.

Oerder, V., F. Cola, V. Echevin, F. Codron, J. Tam, and A. Belmadani, 2015: Peru-Chile upwelling dynamics under climate change. *J. Geophys. Res. Oceans*, **120**, 1151–1172, doi:10.1002/2014JC010299.

Rykaczewski, R. R., J. P. Dunne, W. J. Sydeman, M. García-Reyes, B. A. Black, and S. J. Bograd, 2015: Poleward displacement of coastal upwelling-favorable winds in the ocean's eastern boundary currents through the 21st century. *Geophys. Res. Lett*., **42**, 6424–6431, doi:10.1002/2015GL064694.

Santos, F., M. Gomez-Gesteira, M. DeCastro, and I. Alvarez, 2012: Differences in coastal and oceanic SST trends due to the strengthening of coastal upwelling along the Benguela current system. *Cont. Shelf Res*. **34**, 79–86, doi:10.1016/j.csr.2011.12.004.

Schneider, W., D. Donoso, J. Garces-Vargas, and R. Escribano, 2017: Water-column cooling and sea surface salinity increase in the upwelling region of sentral-south Chile driven by a poleward displacement of the South Pacific High. *Prog. Oceanogr.*, **153**, 16–23, doi:10.1016/j.pocean.2016.11.004.

Sousa, M. C., I. Alvarez, M. deCastro, M. Gomez-Gesteira, and J. M. Dias, 2017: Seasonality of coastal upwelling trends under future warming scenarios along the southern limit of the Canary upwelling system. *Prog. Oceanogr.*, **153**, 16–23, doi:10.1016/j.pocean.2017.04.002.

Sui, C.-H., P.-H. Chung, and T. Li, 2007: Interannual and interdecadal variability of the summertime western North Pacific subtropical high. *Geophys. Res. Lett.*, **35**, doi:10.1029/2006GL029204.

Vizy, E. K., K. H. Cook, J. Crétat, and N. Neupane, 2013: Projections of a wetter Sahel in the 21st century from global and regional models. *J. Climate*, **26**, 4664–4687, doi:10.1175/JCLI-D-12-00533.1.
Vizy, E. K., and K. H. Cook, 2016: Understanding long-term (1982-2013) multi-decadal change in the equatorial and subtropical South Atlantic climate. *Climate Dyn.*, **46**, 2087–2113, doi:10.1007/s00382-015-2691-1.
Vizy, E. K., K. H. Cook, and X. Sun, 2018: Decadal change of the south Atlantic ocean Angola-Benguela frontal zone since 1980. *Climate Dyn.*, doi:10.1007/s00382-018-4077-7.
Wang, D., T. C. Gouhier, B. A. Menge, and A. R. Ganguly, 2015: Intensification and spatial homogenization of coastal upwelling under climate change. *Nature*, **518**, 390–394, doi:10.1038/nature14235.
Xiu, P., F. Chai, E. N. Curchitser, and F. S. Castruccio, 2018: Future changes in coastal upwelling ecosystems with global warming: The case of the California current system. *Sci. Rep.*, **8**, doi:10.1038/s41598-018-21247-7.
Zhou, T., and Coauthors, 2009: Why the Western Pacific subtropical high has extended westward since the late 1970s. *J. Climate,* doi:10.1175/2008JCLI2527.1.
Zwiers, F. W., and H. von Storch, 1995: Taking serial correlation into account in tests of the mean. *J. Climate*, **8**, 336–351, doi:10.1175/15200442(1995)008.

In recognition of 20 years of advancing climate research, members of the US CLIVAR community are sharing some of their thoughts on the value of the program, stories and achievements from over the years, and hopes for the future.

Watch
20th Anniversary Video

Read
Community Testimonials

ANNOUNCEMENTS

Welcome two new US CLIVAR Working Groups

Large "Initial-Condition" Earth System Model Ensembles

The intent of the working group is to spearhead a dedicated effort across the national and international climate communities to advance progress on identifying anthropogenic influences on weather and climate amidst the "noise" of internal variability.

Observations and Modeling of Water Isotopes in the Climate System

The intent of the working group is to characterize and utilize water isotope ratios as a climate variable, through a combination of modern observations, past climate records, and model simulations

Variations Webinar

Expansion of the Tropics

Wednesday, June 27
1:00 - 2:00 PM ET

Featuring authors from this edition:
Nick Davis (CIRES/NOAA ESRL)
Isla Simpson (NCAR)
Jacob Scheff (U. North Carolina, Charlotte)

CLICK HERE TO JOIN!

usclivar.org
uscpo@usclivar.org
twitter.com/usclivar

US Climate Variability and Predictability (CLIVAR) Program
1201 New York Ave. NW, Suite 400
Washington, DC 20005
(202) 787-1682

US CLIVAR acknowledges support from these US agencies:

This material was developed with federal support of NASA and NSF (AGS-1502208), NOAA (NA16OAR4310253), and DOE (DE-SC0016332). Any opinions, findings, conclusions, or recommendations expressed in this material are those of the authors and do not necessarily reflect the views of the sponsoring agencies.